16 State House Station
Augusta, Maine 04333

MaineDOT

Transportation Research Division

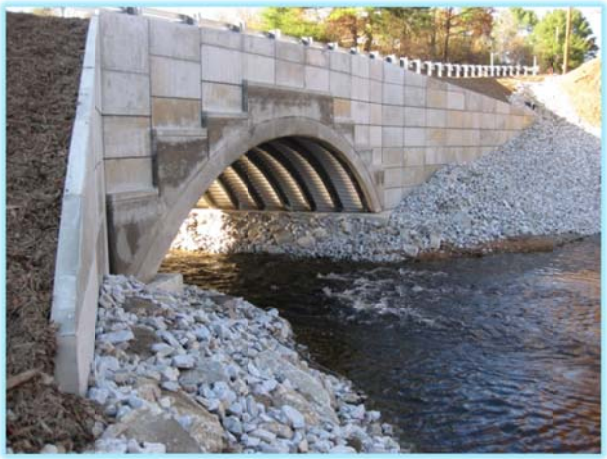

Technical Report 14-03

Bridge-in-a-Backpack™

Task 2: Reduction of costs through design modifications and optimization

Final Report – Task 2, September 2011

Technical Report Documentation Page

1. Report No. ME 14-03	2.	3. Recipient's Accession No.
4. Title and Subtitle Bridge-in-a-Backpack™ Task 2: Reduction of costs through design modifications and optimization		5. Report Date September 2011 6.
7. Author(s) Harold Walton Bill Davids Ph.D P.E. Josh Clapp P.E. Keenan Goslin P.E. Roberto Lopez-Anido Ph.D, P.E.		8. Performing Organization Report No. AEWC Report Number 12 – 08.814
9. Performing Organization Name and Address University of Maine – Advanced Structures and Composites Center		10. Project/Task/Work Unit No. Project 17681.00 - Task 2 11. Contract © or Grant (G) No. Contract # 2010*3692
12. Sponsoring Organization Name and Address Maine Department of Transportation		13. Type of Report and Period Covered 14. Sponsoring Agency Code
15. Supplementary Notes		

16. Abstract (Limit 200 words)

The cost effective use of FRP composites in infrastructure requires the efficient use of the composite materials in the design. Previous work during the development phase and demonstration phase illustrated the need to refine the design methods for portions of these types of structures. Three parts were included in this task aimed at reducing costs through design modifications and optimization. They include improvements to the soil-structure interaction analysis methods, identification and/or design of a stronger decking material to span between the arches, and other advanced modeling tools. In the case of advanced modeling tools, it has been shown that a very important portion of the loading history of the arches includes the concrete filling of the tubes during construction. A majority of this report explains the evaluation and modeling of unfilled, hollow tubes to create a knowledge base and design methodology where the tubes could be safely analyzed for filling loads.

17. Document Analysis/Descriptors Arch bridges, concrete filled FRP tubes, Bridge-in-a-Backpack		18. Availability Statement	
19. Security Class (this report)	20. Security Class (this page)	21. No. of Pages 170	22. Price

Bridge-in-a-Backpack™
Task 2: Reduction of costs through design modifications and optimization

AEWC Project 814
PIN 017681.00

Prepared for:
Dale Peabody
Maine Department of Transportation
Office of Safety, Training, and Research
16 State House Station
Augusta, ME 04333
(207) 624-3305

AEWC Report Number
12 – 08.814

September 27th, 2011

Prepared by:

Harold Walton
Bill Davids Ph.D P.E.
Josh Clapp P.E.
Keenan GoslinP.E.
Roberto Lopez-Anido Ph.D P.E.

An ISO 17025 accredited testing laboratory
Accredited by International Accreditation Service

AEWC Advanced Structures & Composites Center
5793 AEWC Bldg
University of Maine
Orono, ME 04469-5793

CONFIDENTIAL

Telephone: 207-581-2123
FAX: 207-581-2074
contactaewc@umit.maine.edu
www.aewc.umaine.edu

This test report shall not be reproduced, except in full, without the written approval of the AEWC Advanced Structures & Composites Center.

Bridge-in-a-Backpack™
Task 2: Reduction of costs through design modifications and optimization

The cost effective use of FRP composites in infrastructure requires the efficient use of the composite materials in the design. Previous work during the development phase and demonstration phase illustrated the need to refine the design methods for portions of these types of structures. Three parts were included in this task aimed at reducing costs through design modifications and optimization. They include improvements to the soil-structure interaction analysis methods, identification and/or design of a stronger decking material to span between the arches, and other advanced modeling tools. In the case of advanced modeling tools, it has been shown that a very important portion of the loading history of the arches includes the concrete filling of the tubes during construction. A majority of this report explains the evaluation and modeling of unfilled, hollow tubes to create a knowledge base and design methodology where the tubes could be safely analyzed for filling loads.

Task 2.1 Simplified Modeling to Assess Soil-Structure Interaction Effects

All applications to date of hybrid FRP concrete arch tubular bridges have been buried structures where transverse decking was placed across the arches to distribute soil loads, dead loads, and live loads to the arches. FRP decking may be used alone or as formwork for reinforced concrete decking. Present structural analysis methods consist of finite element (FE) models that utilize 2D Euler-Bernoulli beam elements to model the arch. Nonlinear moment-curvature relationships can be included. The axial and bending stiffnesses of the concrete deck, if present, are neglected. Soil loads are applied by assuming a constant lateral earth pressure coefficient, K (taken as the at-rest coefficient, K_o), to relate horizontal and vertical soil pressures.

This document is intended to summarize the work that was performed by the University of Maine AEWC Advanced Structures and Composites Center (AEWC) in collaboration with Advanced Infrastructure Technologies (AIT) to develop new structural analysis software to analyze buried arch bridges that accounts for unbalanced backfilling and the potentially beneficial restraining effect of the compacted backfill on the arches. All routines were written in MATLAB (MathWorks 2009) so that the user has full control

This test report shall not be reproduced, except in full, without the written approval of the AEWC Advanced Structures & Composites Center.

over the analysis and may easily make changes to the analysis routines. The software incorporates four key capabilities:

1. The effect of staged construction was simulated by applying soil lifts sequentially on alternating sides of the arch.
2. A nonlinear soil constitutive relationship was incorporated by adding soil springs to the model corresponding to each layer of soil after it is placed.
3. Recognizing that the arches behave as stiff ribs supporting the more flexible deck, which may significantly affect soil-structure interaction, the decking was explicitly modeled using transverse elements perpendicular to the plane of the arch.
4. The effect of the axial and bending stiffness of the concrete deck, if present, in the longitudinal (span) direction was included in the model.

The net effect of these key features of the analysis methodology was investigated by modeling the backfilling of an example bridge which is proposed for construction in the near future at the time of this report. This allowed realistic parameters to be considered in a practical design scenario. Throughout this document references are made to this particular bridge project referred to as the Ellsworth Bridge. Details describing the example bridge and in general the work that was to be performed as part of the contract can be found in Clapp (2011).A collection of content specifically related to the programming aspect of the project can be found in Clapp (2011) as well.

Finite element model

Three-dimensional (3D) elements were utilized in order to capture the effect of decking flexibility in the transverse direction (spanning between arches). A schematic view of the finite element mesh is shown in Figure 1. Three element types were used: arch elements (also includes longitudinal decking stiffness if applicable), transverse decking elements, and soil spring elements. Nonlinear 3D Euler-Bernoulli beam elements were used to model the arch in the longitudinal direction as well as the decking in the transverse direction. If a concrete deck is present, the stiffness of the deck in the longitudinal direction is added to the stiffness of the arch to arrive at the total non-composite stiffness for these elements. For this study, a cracked section was considered for the concrete deck in both the longitudinal and transverse directions. Soil spring elements were based on a compression-only constitutive relationship that is discussed later. The arch boundary conditions were taken as fully fixed at the ends, although other boundary conditions can be specified. Loads were applied to nodes defining the transverse decking elements and were then transferred to the arch.

This test report shall not be reproduced, except in full, without the written approval of
the AEWC Advanced Structures & Composites Center.

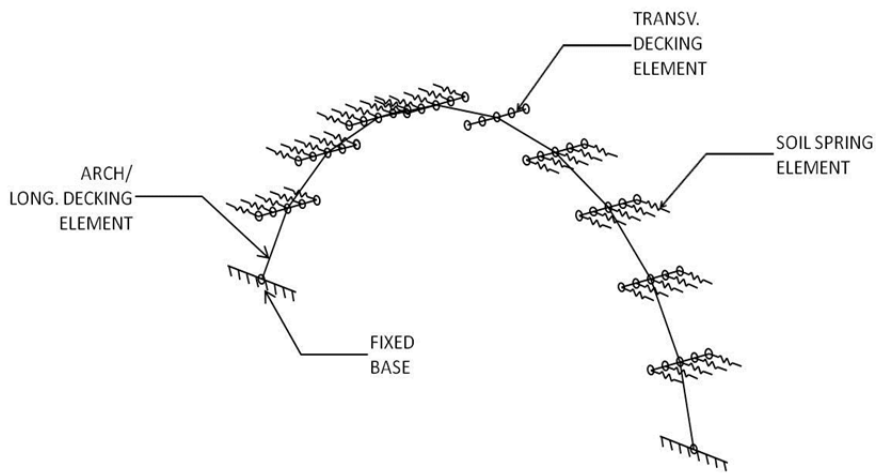

Figure 1 – Schematic 3D View of FE Mesh (Coarse Mesh Shown for Clarity)

Arch and Longitudinal Decking Elements

General nonlinear 3D Euler-Bernoulli beam elements were used to model the arch, although only in-plane deflections/member forces occurred since the arch was not subjected to out-of-plane loads in this study. The in-plane tangent bending stiffness, EI, and bending moment for the arch are a function of curvature and axial load level. These values were interpolated from relationships provided by AIT. If a concrete deck is present, it is also necessary to account for the in-plane longitudinal bending and axial stiffness of this layer. In this study, two different values of EI corresponding to cracked sections were used depending on whether positive or negative bending was occurring. This was necessary since the location of reinforcement was non-symmetric through the depth of the deck. It is also possible for the user to specify a generic moment-curvature relationship for the decking in the longitudinal direction. The area used to calculate axial stiffness, EA, of the decking was taken as the full uncracked cross-sectional area of the concrete. Throughout analyses the total axial load was split into arch and decking components proportionally to their stiffnesses and only the arch component was used when interpolating for its bending stiffness and moment.

Transverse Decking Elements

General and specialized nonlinear 3D Euler-Bernoulli beam elements were used to model the decking in the transverse direction. These elements were only intended to capture the effect of transverse bending, which leads to variable soil pressures across the length of the decking elements. Longitudinal bending and axial stiffness of the decking was included with the arch elements. A single row of decking elements, which can contain any even number of elements, extends from –s/2 to s/2, where s is the center-to-center

This test report shall not be reproduced, except in full, without the written approval of
the AEWC Advanced Structures & Composites Center.

spacing of the arches. The local coordinate system [x′,y′,z′] of the decking elements is defined in Figure 2. The global coordinate system [X,Y,Z] is also shown for reference. Note that the x′ axis is parallel to the Z axis. For each element, the z′ axis was taken as being parallel to a line connecting the two adjacent arch nodes, as indicated by line A-B in Figure 2. The y′ axis was taken as perpendicular to the x′ and z′ axes. The actual bending stiffness of the deck was used for bending about the z′ axis. A large bending stiffness was applied for bending about the y′ axis to effectively prevent displacements in the x′-z′ plane. To model the symmetric bending of the decking, rotations about the z′ axis at each end of the decking must be prevented. Specialized elements were used to achieve this rotational restraint at coordinates Z = –s/2 and Z = s/2. This boundary condition was taken into account in the element formulation to arrive at a consistent element stiffness matrix, and it was not necessary to apply additional constraints in the model. General 3D Euler-Bernoulli beam elements were used for all other decking elements.

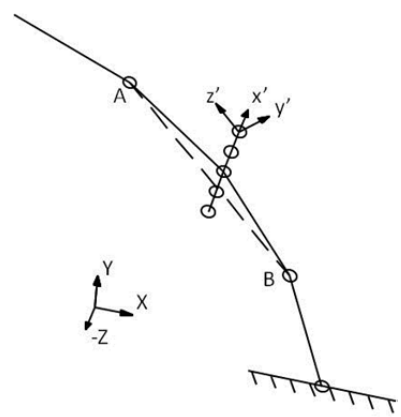

Figure 2 – Definition of Local Coordinate System for Transverse Decking Elements

Soil Spring Elements

Soil spring elements were oriented horizontally and only carried compressive axial loads. The axial load level F_{spring} depends on the tributary horizontal area A_h, the vertical pressure σ_v due to overburden and other loads, and the lateral earth pressure coefficient K as shown in Equation 1 below. Here, A_h was taken as the product of half of the elevation difference between the two adjacent nodes along the length of the arch and the z-spacing of decking nodes (or z-spacing/2 for nodes at the planes of symmetry).

This test report shall not be reproduced, except in full, without the written approval of
the AEWC Advanced Structures & Composites Center.

$$F_{spring} = A_h \times \sigma_v \times K$$ Equation 1

Stiffness was estimated by using a forward difference approximation where a small deflection was applied. The tributary area for a particular element remained constant throughout the analysis, whereas σ_v and K changed as a function of additional loading and deflections, respectively. The lateral earth pressure coefficient K was defined based on Figure 3 below (see 'UMaine Model'), where deflections away from the soil were taken as positive. A curve reproduced from National Cooperative Highway Research Program (NCHRP 1991) is also shown for comparison. Note that the UMaine Model is just a simplified quadrilinear version of the NCHRP (1991) curve defined by the three pressure coefficients, except that K_o was taken as 0.45. This value represents a compromise between the NCHRP (1991) value of 0.4 and the value recommended by Maine DOT for culvert design of 0.47. Precedent for this approach can be found in literature on integral abutment bridges (Faraji et al. 2001; Ting and Faraji 1998) and in design procedures for earth retaining structures (USACoE 1994). Note that the UMaine model yields much softer behavior for the soil springs than the NCHRP curve, which was believed to be conservative. We note here that the MATLAB code developed as part of this work is quite general, and should permit alternative soil spring load-deformation relationships to be implemented fairly easily.

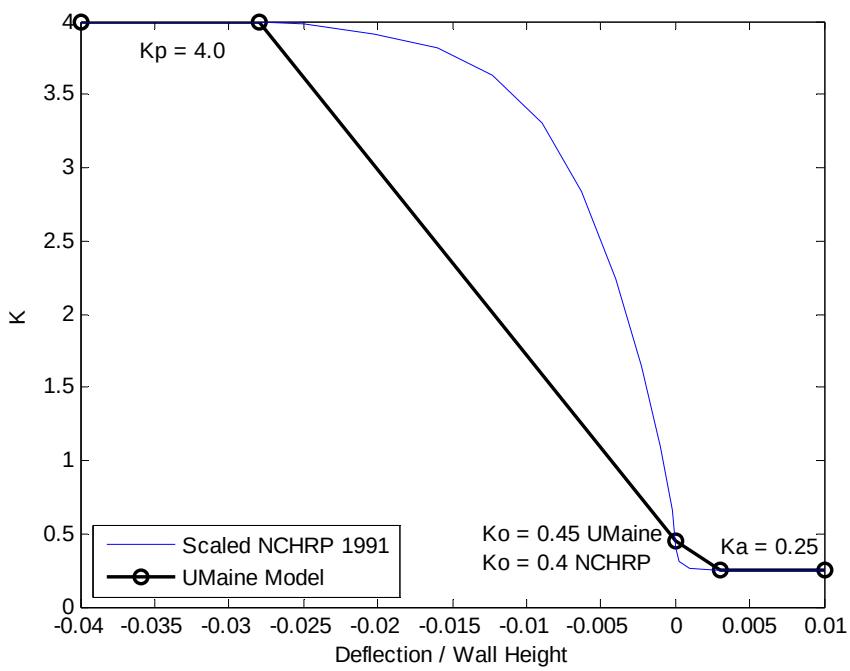

This test report shall not be reproduced, except in full, without the written approval of the AEWC Advanced Structures & Composites Center.

Figure 3 – Lateral Earth Pressure Coefficient as a Function of Relative Movement after NCHRP (1991) for Medium-Dense Backfill

The wall height for the example case was taken as the height of the arch, or 14 ft., which implies that deflections of approximately 0.5 in. away from and 4.7 in. into the soil are necessary to achieve the active and passive states, respectively. These deflections were defined relative to the horizontal displacement of the arch at the location of the spring after the applicable soil lift was applied (i.e. after a lift was placed that first caused a particular soil spring to be buried, the initial relative deflection for this soil spring was zero).

Consideration of staged construction

In the field, the backfilling process is performed after the arches are placed and decking is installed. Generally, based on recent bridge construction projects, the backfill is placed in lifts that do not exceed 12 in. in height and lifts are placed sequentially on alternating sides of the arch. Each lift is compacted before the next lift is placed. It was assumed for the analyses described in this document that a lift is in the at-rest state once it has been placed and compacted. After this point the state depends on deflections. Lifts were applied in 12 in. increments on alternating sides of the arch since this was believed to be the maximum differential between lifts on opposing sides of the arch during construction i.e. the scenario that causes the largest amount of side-sway. (The program allows lift heights of other than 12 in. to be specified.) The algorithm for the staged construction procedure, which takes place after the self-weight of arch and decking components are applied, was as follows:

1. Apply a new lift of soil.
    a. Horizontal loads corresponding to the at-rest lateral earth pressure coefficient K_o are applied within the region of this lift in addition to vertical loads applied in all applicable regions.
    b. Element shape functions are used to calculate statically equivalent nodal loads for vertical and horizontal soil pressures that vary linearly over the length of an element.
    c. The tributary distance in the z-direction is taken as the z-spacing of decking elements (or z-spacing/2 for nodes at the planes of symmetry).
2. Adjust the vertical pressure for any lifts that are below the new lift.
3. Re-calculate the stiffness of each soil spring based on the additional vertical pressure as well as the change in relative deflection.
4. Utilize a nonlinear Newton-based solver to determine the position of equilibrium, while continually updating the stiffness of nonlinear elements in the model including the soil springs.

This test report shall not be reproduced, except in full, without the written approval of the AEWC Advanced Structures & Composites Center.

5. After a solution has been obtained, activate any springs that were buried by the lift that was just applied.
6. Set the zero relative displacement position of the newly activated springs to be at the X-coordinate of the current deflected position. This 'zero' position will be retained for all future load steps.
7. Repeat 1-6 until all lifts are applied.
8. Apply additional loads such as dead load of the wearing surface and vehicle live loads.

Consideration of live loads

After backfilling was completed, the next step was to apply the wearing surface and then live loads were applied. Both a uniform lane load and a vehicular live load were considered per AASHTO. In this software, this process was broken into three steps: 1) dead load of the wearing surface DW, 2) AASHTO lane load, and 3) AASHTO vehicular loading. All analyses resume from the point at which the previous step was completed. For example, the DW analysis starts from the point at which the last backfilling step was applied. This was necessary since the principle of superposition does not apply for nonlinear analyses. The results of step (3) minus the results of step (1) represented the total effect of live loading. The lane load was applied separately from the live load only because it is a constant load and therefore it is not necessary to re-apply it for various truck positions in an envelope-type analysis. This may result in reduced computational time.

The loads and vertical stresses associated with the dead load of the wearing surface and the uniform lane load were simply based on tributary area. On the other hand, the loads for the vehicular live load were calculated using the integral solution to the Boussinesq vertical stress equation. The vertical stress used to calculate soil spring forces due to vehicular live loads was taken as the calculated force divided by the tributary area.

Specific parameters used for analyses

All analyses conducted as part of this study were based on expected values for the proposed Ellsworth Bridge Project. A majority of these parameters were directly provided by AIT and are summarized in Table 1. Parameters not directly provided were calculated/ estimated based on drawings and other information provided by AIT. Supporting calculations are provided in Appendix A.

This test report shall not be reproduced, except in full, without the written approval of the AEWC Advanced Structures & Composites Center.

Table 1 – Specific Parameter Values for Analyses

Description	Variable	Units	Decking	
			Concrete	FRP
Diameter of CFRP tube	diam	in	11.8	
Rise of arch centerline	rise	ft	14	
Span of arch centerline	span	ft	34.33	
Depth of backfill above arch crown	depth_crown	ft	Variable, 3-12.5	
Depth of wearing surface	DW_depth	in	3	
Equivalent deck thickness for self-weight calculation	deck_thick	in	7.8	0.31
Arch spacing	spacing	in	60	
Strength of concrete in the arch	Fpc	psi	5000	
Soil density	rho	pcf	125	
Wearing surface density	rho_asphalt	pcf	140	
Design truck axle	Axle_space		Short	
Number of lanes loaded	num_lanes		2	
All load factors			1	
Number of arch elements	numels		60	
Number of deck elements (per section)	num_deck		8	
Effective height for which to apply soil springs	H_effective	ft	14	
Elastic modulus of deck	E_deck	ksi	3759	4200
Area of concrete deck, long.	A_deck	in^2/in	5	NA
Positive bending moment of inertia, long.	I_pos	in^4/in	0.592	NA
Negative bending moment of inertia, long.	I_neg	in^4/in	0.066	NA
Area of concrete deck, trans.	A_deck	in^2/in	7.68	0.303
Positive & negative bending moment of inertia, trans.	I_deck	in^4/in	3.2	0.93
Effective radial distance from arch centerline to soil	t_deck	in	14.4	7.9
Lateral pressure coefficient, active	Ka		0.25	
Lateral pressure coefficient, at-rest	Ko		0.45	
Lateral pressure coefficient, passive	Kp		4	

This test report shall not be reproduced, except in full, without the written approval of the AEWC Advanced Structures & Composites Center.

Deflection/H_effective, active	delta_Ka		0.003
Deflection/H_effective, passive	delta_Kp		0.028

The geometry of the circular arc-segment was provided by AIT. Another arch geometry, referred to as the "Bebo" or "ConSpan" arch was also provided by AIT. The geometry of this arch is based on an elliptical shape. It is steeper near the supports and flatter near midspan as compared to a circular arc-segment arch. The total span and rise were held constant. An intermediate multi-radius geometry was also considered. This was a symmetric 3-radius arch with interior (around midspan) curve defined by a radius of about 19.6 ft and included angle of about 77.4 degrees. The exterior (near supports) curves of this geometry were defined by a radius of about 13.3 ft and included angle of about 48.4 degrees. All three geometries are shown in Figure 4.

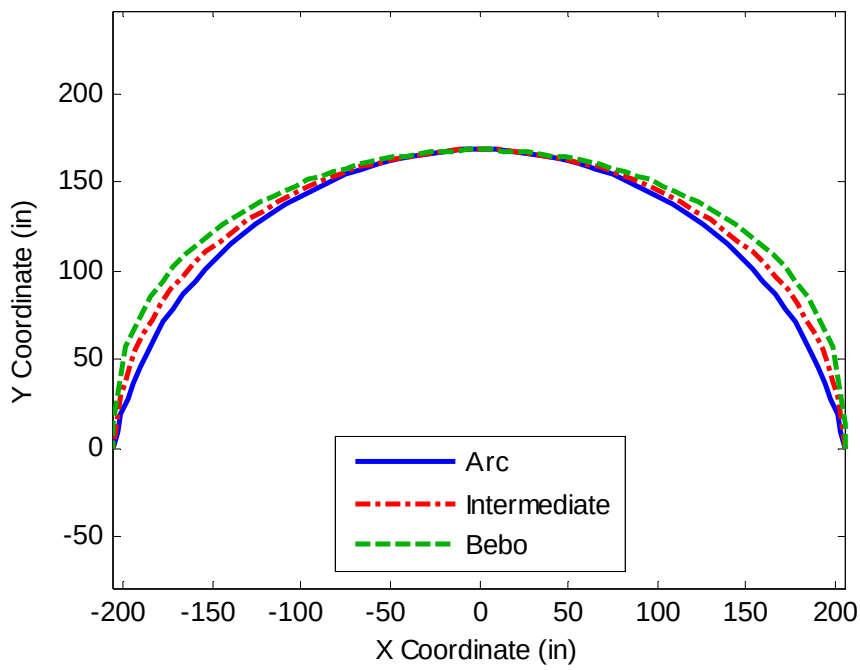

Figure 4 – Geometric Configurations for Analyses

Results: effect of staged backfilling

Staged backfilling affects analysis results in several ways: 1) alternating soil lifts result in side-sway and non-symmetric response about midspan; 2) staged backfilling allows

This test report shall not be reproduced, except in full, without the written approval of
the AEWC Advanced Structures & Composites Center.

lateral earth pressure coefficients other than the at-rest coefficient to be rationally considered, which generally reduces critical response values; and 3) staged backfilling allows the structural response to be tracked throughout the construction period, which is important if the greatest response occurs prior to the final backfilling step.

The effect of staged backfilling was examined by running the matrix of analyses shown in Table 2. Three different arch bending stiffness relationships were considered, one of which utilized the nonlinear moment-curvature relationship provided for the arch tubes of this study. The others were linear-elastic relationships intended to provide approximate bounds on the response that would be expected. Both FRP decking and concrete decking were considered. The concrete decking is placed on top of another type of FRP decking in actual bridge applications, but this type of FRP is much softer than the FRP decking that would be used instead of concrete, and its stiffness was neglected in analyses. Three different levels of backfilling were considered: 3, 6, and 12.5 ft. The 3 ft and 6 ft depths are similar to actual values that have been used for recently constructed bridges. The 12.5 ft depth is the specified depth for the proposed Ellsworth Bridge. All results shown here are for service (unfactored) loads.

Results of analyses are presented in Figure 5 through Figure 9 below for both types of decking and also for both arch moment and total foundation thrust. Envelope arch moments are presented, meaning that the values represent the maximum/minimum values for any point along the length of the arch at a particular load step (average backfill elevation).

Table 2 Matrix of Analyses to Examine the Effect of Staged Backfilling

Arch Bending Stiffness	**Decking**	**Backfill Depth Above Centerline of Arch Crown (ft)**
Nonlinear	Concrete	3
Linear, Uncracked Section	FRP-only	6
Linear, Cracked Section	--	12.5

This test report shall not be reproduced, except in full, without the written approval of
the AEWC Advanced Structures & Composites Center.

Envelope Arch Moments

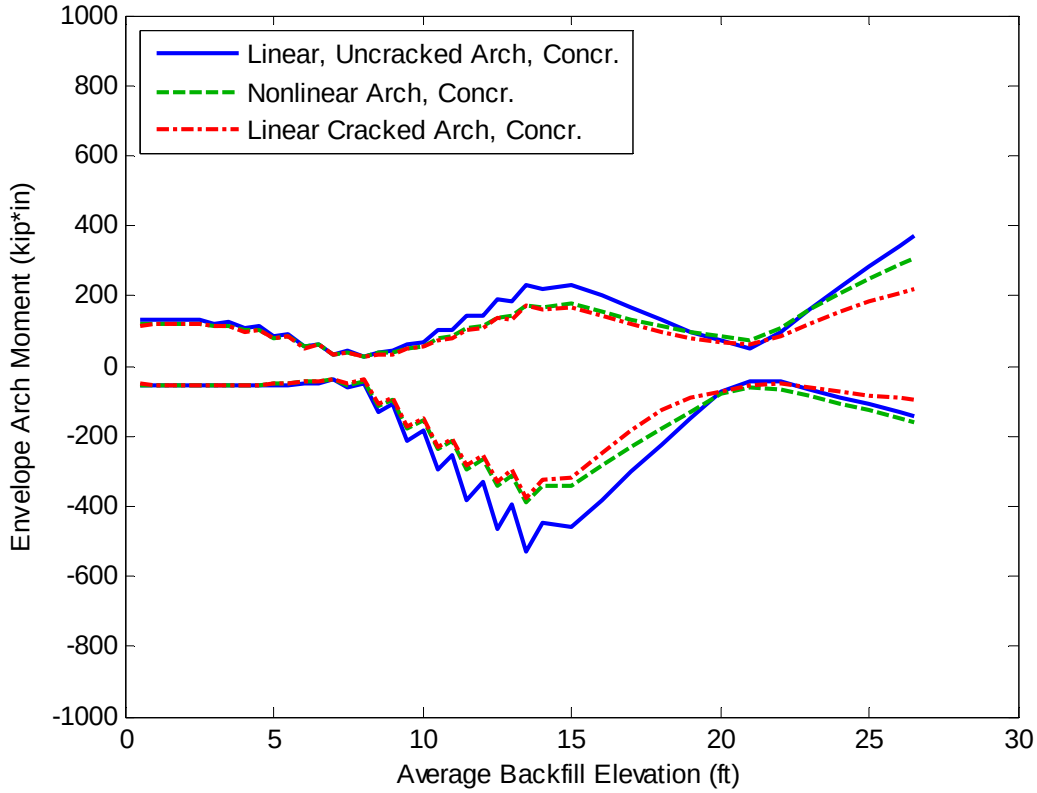

Figure 5 – Backfilling Envelope Arch Moment for Various Arch Bending Stiffness Relationships, Concrete Deck

This test report shall not be reproduced, except in full, without the written approval of the AEWC Advanced Structures & Composites Center.

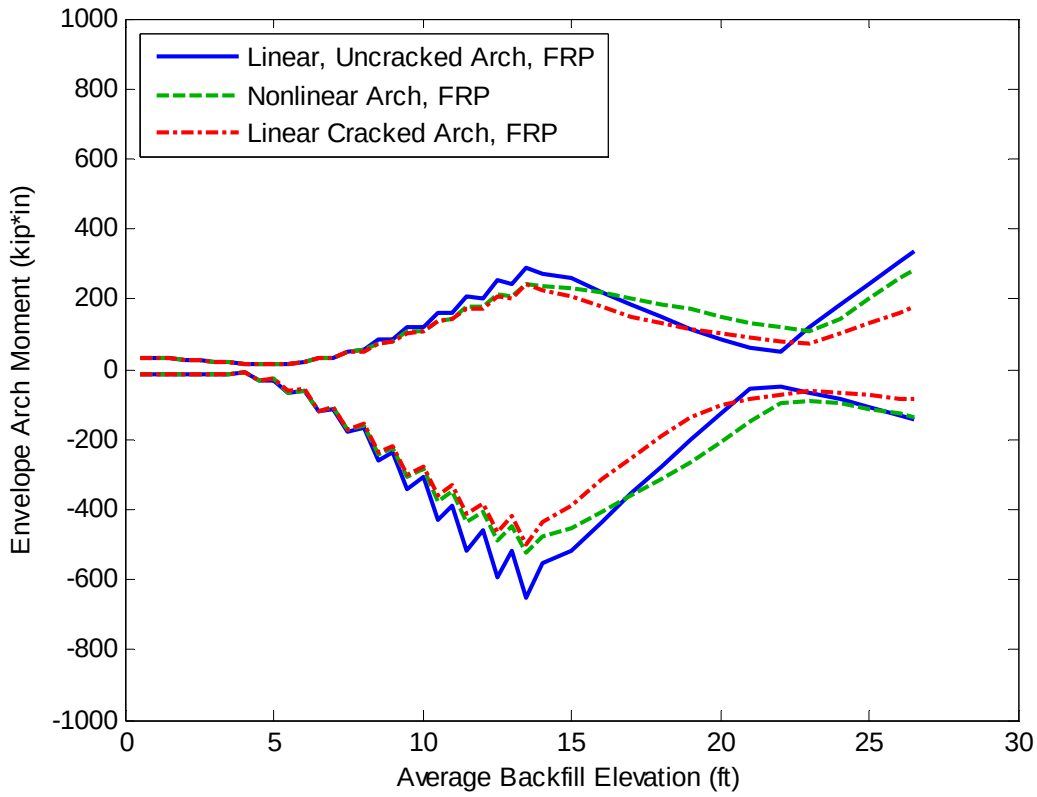

Figure 6 – Backfilling Envelope Arch Moment for Various Arch Bending Stiffness Relationships, FRP Deck

As shown in Figure 5 and Figure 6, the response of the nonlinear arch generally falls between those of the two corresponding linear models for arch bending moment. Generally the arch moments reach a peak at some point during construction near the point at which the backfill elevation approaches the height of the arch (14 ft). After which the magnitude of the moments generally decreases until the backfill elevation is around 21-22 ft, and then increases again. Thus, the critical construction moment may occur prior to the last load step, depending on the final backfill elevation.

The increased moment at elevations near 14 ft. stems from the fact that the alternating soil lifts cause side-sway and increased moments. The side-sway is depicted graphically in Figure 7 for the model with nonlinear arch bending stiffness relationship and a concrete deck. The original position of the arch is outlined in black. The deformed shape is indicated by the thick blue line (deflections are scaled by a factor of 10). It is apparent

This test report shall not be reproduced, except in full, without the written approval of the AEWC Advanced Structures & Composites Center.

from this illustration that the deflections (and resulting moments) are much greater as the backfill level is near the top of the arch. However, at the final grade elevation, the deflections are relatively small and many of the soil springs (not shown) have increased in stiffness (i.e. $K > K_o$). This stiffness of the soil is expected to reduce live load moments in the arch.

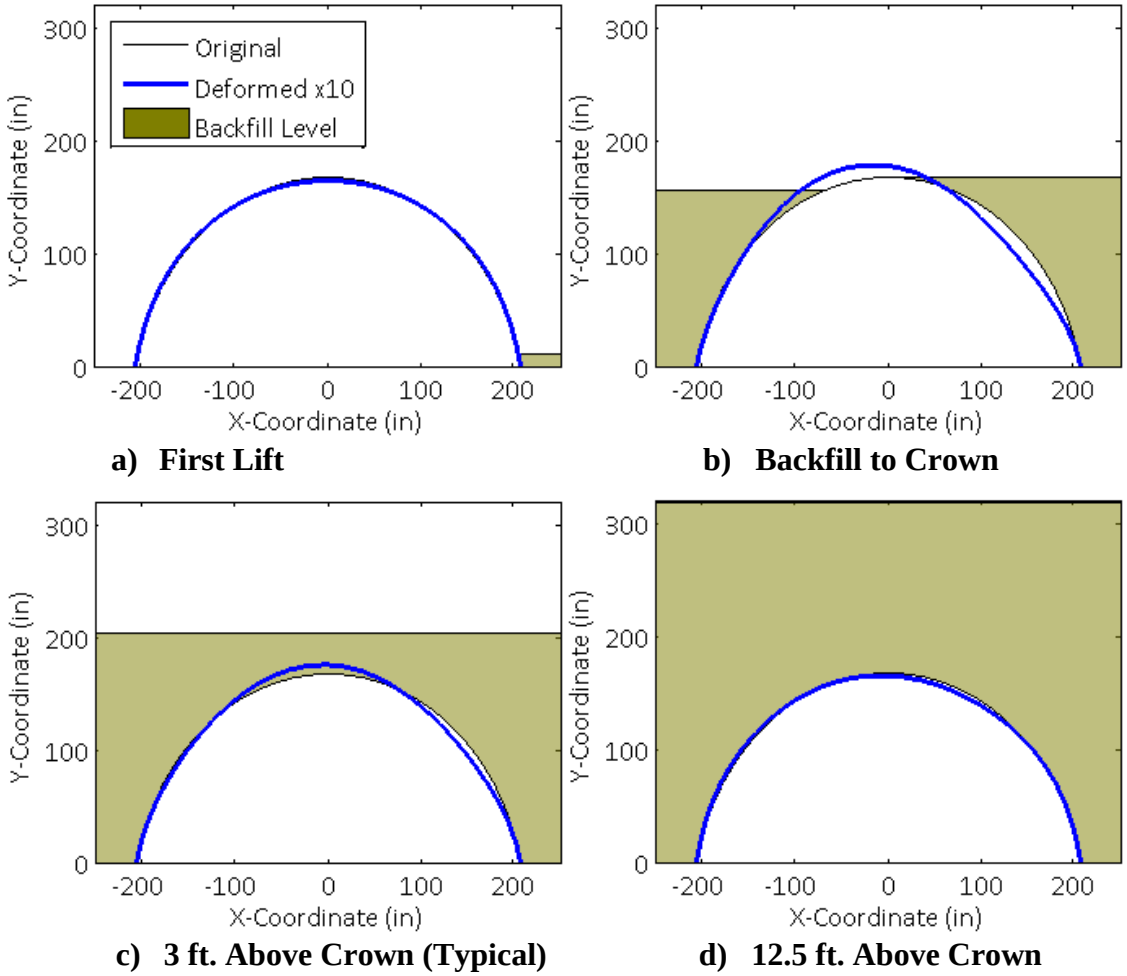

Figure 7 – Deflected Shape of the Arch at Various Backfill Levels, Nonlinear Arch Bending Stiffness, Concrete Deck

This test report shall not be reproduced, except in full, without the written approval of the AEWC Advanced Structures & Composites Center.

Outward Foundation Thrust

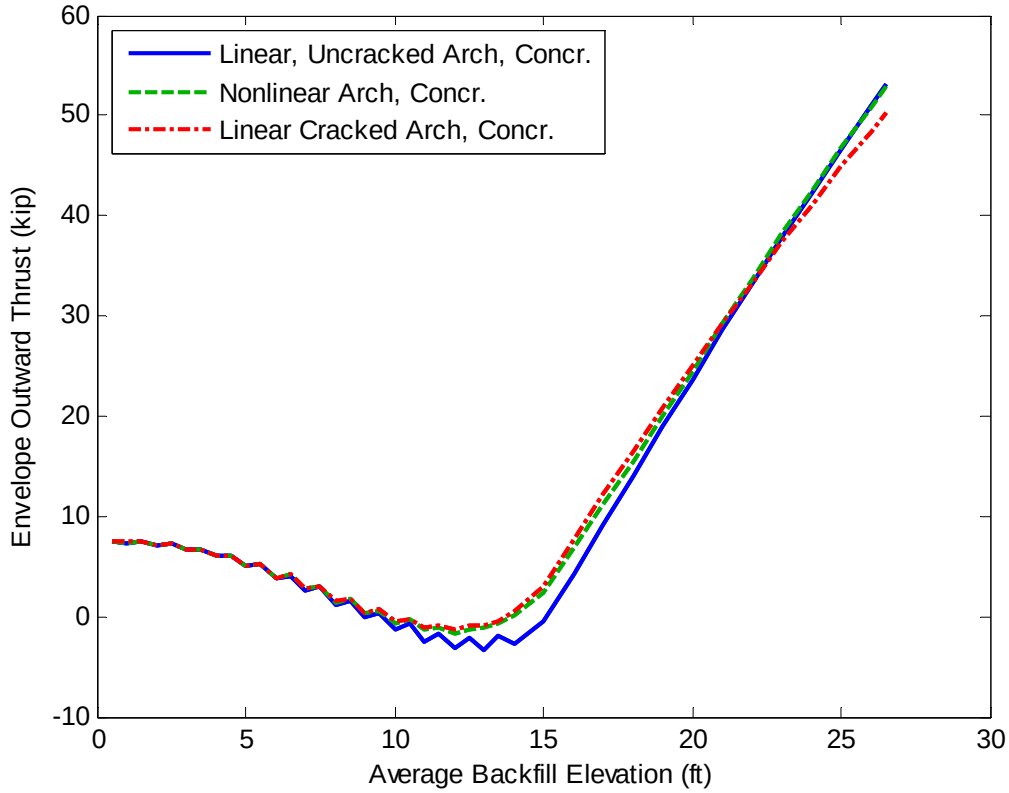

Figure 8 – Backfilling Envelope Outward Thrust for Various Arch Bending Stiffness Relationships, Concrete Deck

This test report shall not be reproduced, except in full, without the written approval of the AEWC Advanced Structures & Composites Center.

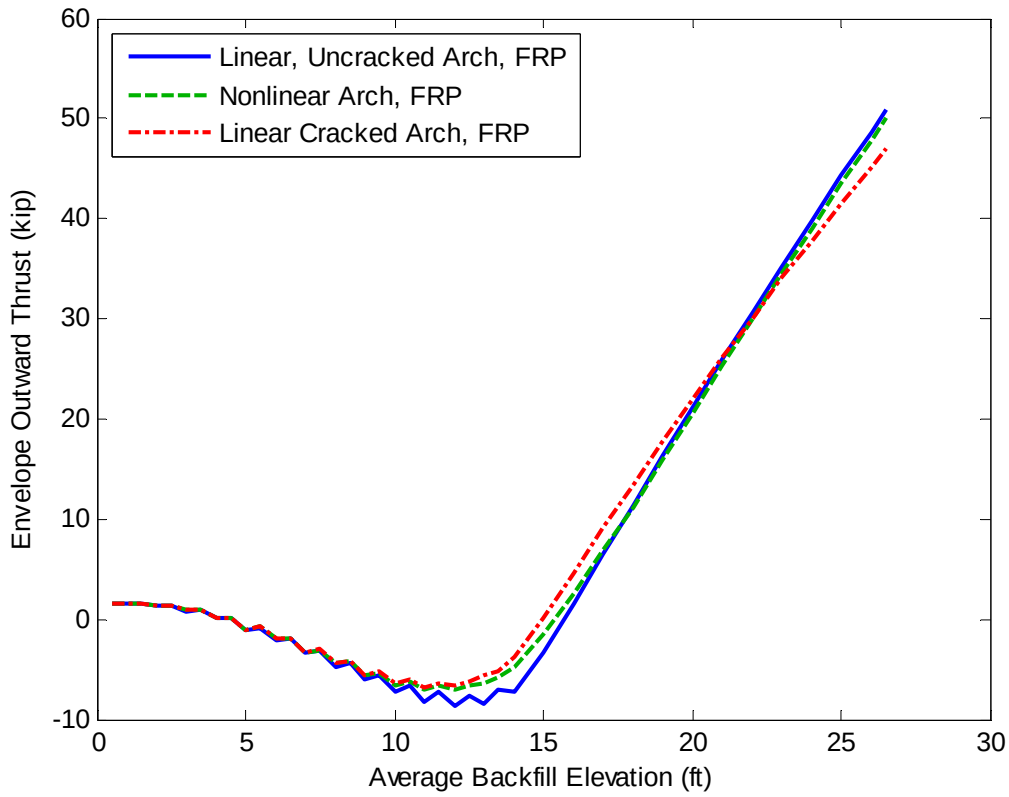

Figure 9 – Backfilling Envelope Outward Thrust for Various Arch Bending Stiffness Relationships, FRP Deck

As shown in Figure 8 and Figure 9, the response of the nonlinear arch again generally falls between the responses of the two corresponding linear models for arch outward thrust. Note that thrust values for the concrete-decked arches are initially much larger than those for FRP-decked arches due to the increased self-weight of the concrete. However, as the backfill elevation exceeds the approximate height of the arch, the thrust forces are dominated by the backfilling loads and both types of decking show similar results. It is important to note that the thrust force reported is not the total horizontal reaction, but rather the horizontal reaction at the base of the arch. The total reaction is the sum of the base reaction plus all of the horizontal spring forces.

This test report shall not be reproduced, except in full, without the written approval of
the AEWC Advanced Structures & Composites Center.

Envelope Arch Axial Load

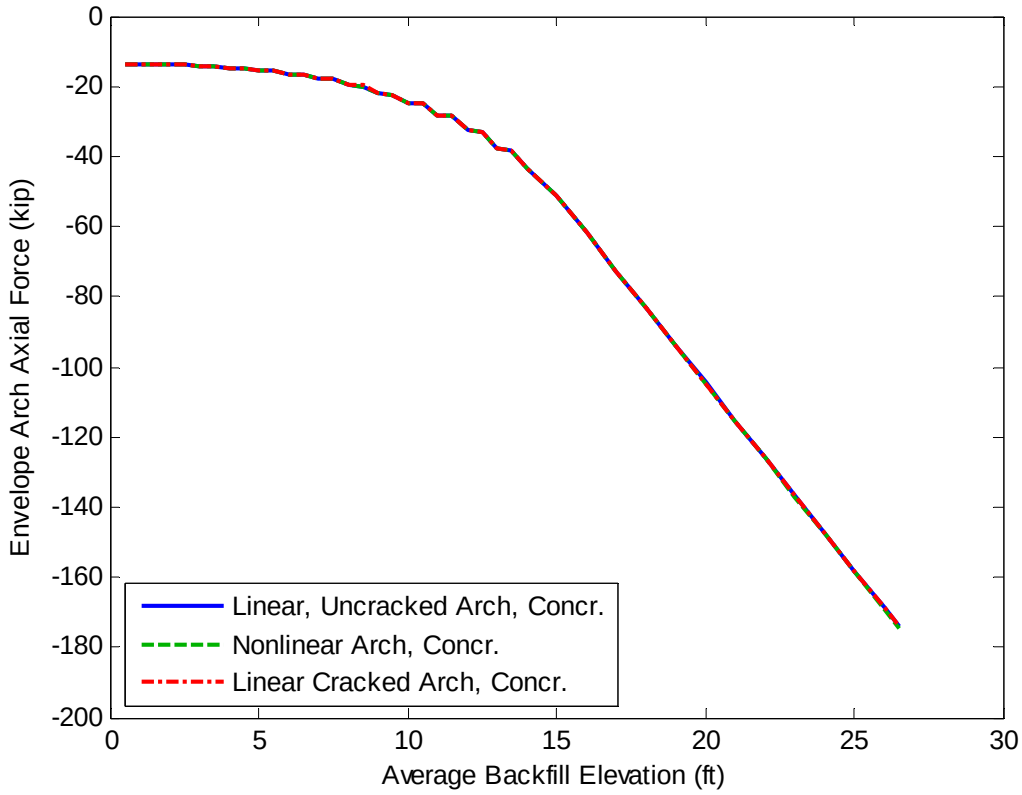

Figure 10– Backfilling Envelope Arch Axial Load for Various Arch Bending Stiffness Relationships, Concrete Deck

This test report shall not be reproduced, except in full, without the written approval of the AEWC Advanced Structures & Composites Center.

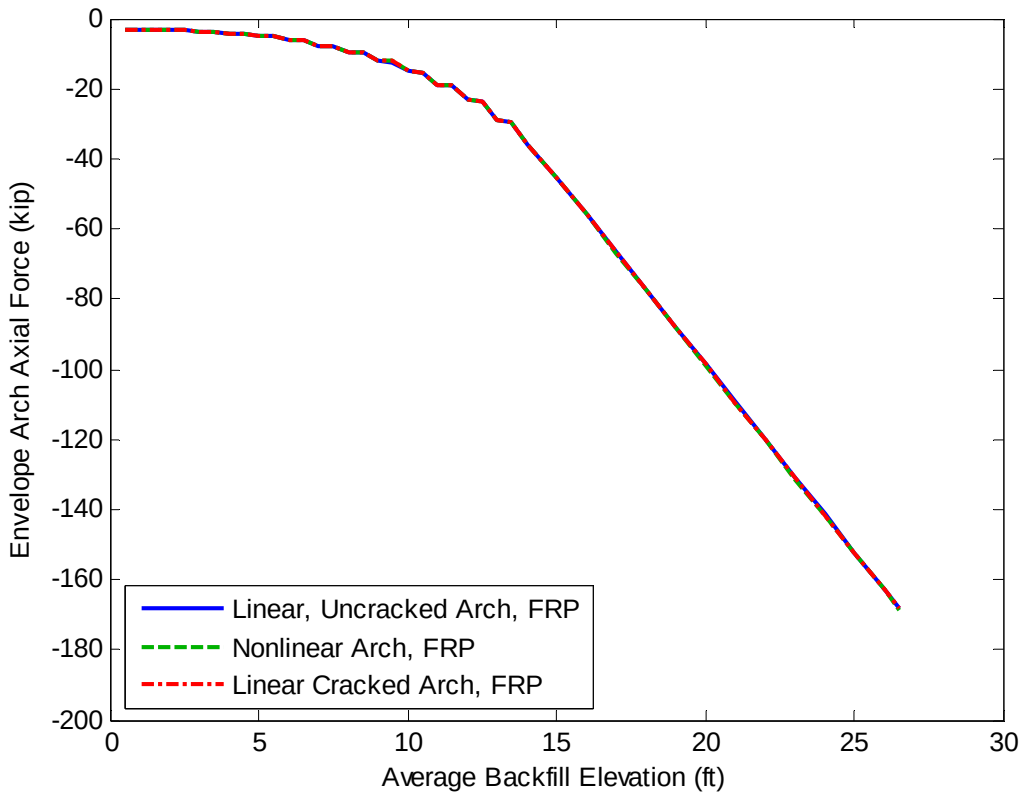

Figure 11 – Backfilling Envelope Arch Axial Load for Various Arch Bending Stiffness Relationships, FRP Deck

As shown in Figure 10 and Figure 11, the axial response of the arch is practically unaffected by the type of relationship used to describe the arch bending stiffness. The magnitude of the axial load in the concrete-decked arches is slightly more than for the FRP-decked arches due to the increased self-weight.

Results: effect of arch geometry

The geometry of the arches has a major effect on the way that the structure responds to a given set of loads. All bridges constructed to-date have utilized circular arc-segment arches. However, this configuration may not be ideal for all applications. Other geometric configurations are possible and have been considered for future projects. For example, one possible configuration is an arch that is relatively steeper near the supports and flatter near midspan as compared to a circular segment arc shape. This shape tends to result in

This test report shall not be reproduced, except in full, without the written approval of the AEWC Advanced Structures & Composites Center.

decreased foundation thrust and increased arch member bending moments. Based on economic factors, the shape of the arch could be optimized to achieve a desired effect. In this study, the effect of arch geometry was investigated by analyzing the three geometric shapes described previously. The matrix of analyses conducted is shown below in Table 3.

Table 3 Matrix of Analyses to Examine the Effect of Arch Geometry

Arch Geometry	Decking
Circular Segment Arc	Concrete
ConSpan Bebo Arch	FRP-only
Multi-radius (Intermediate)	--

Envelope Arch Moments

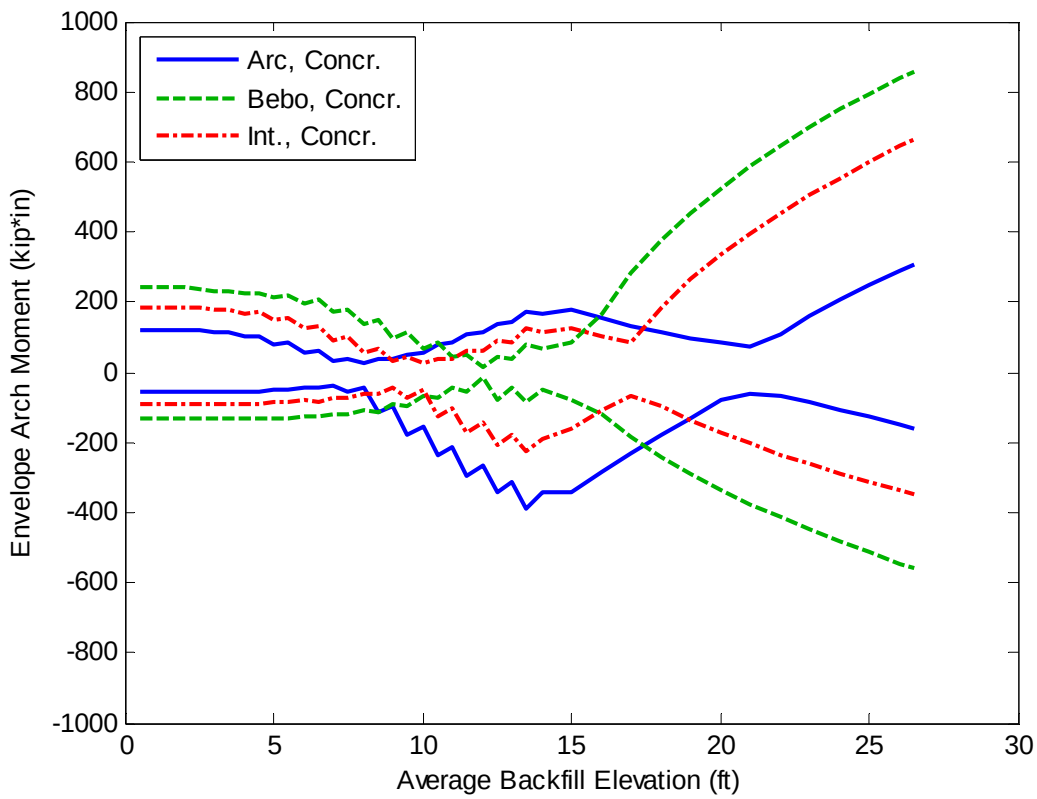

This test report shall not be reproduced, except in full, without the written approval of the AEWC Advanced Structures & Composites Center.

Figure 12 – Backfilling Envelope Arch Moments for Various Geometric Configurations, Concrete Deck, 12.5 ft of Total Fill Above the Crown

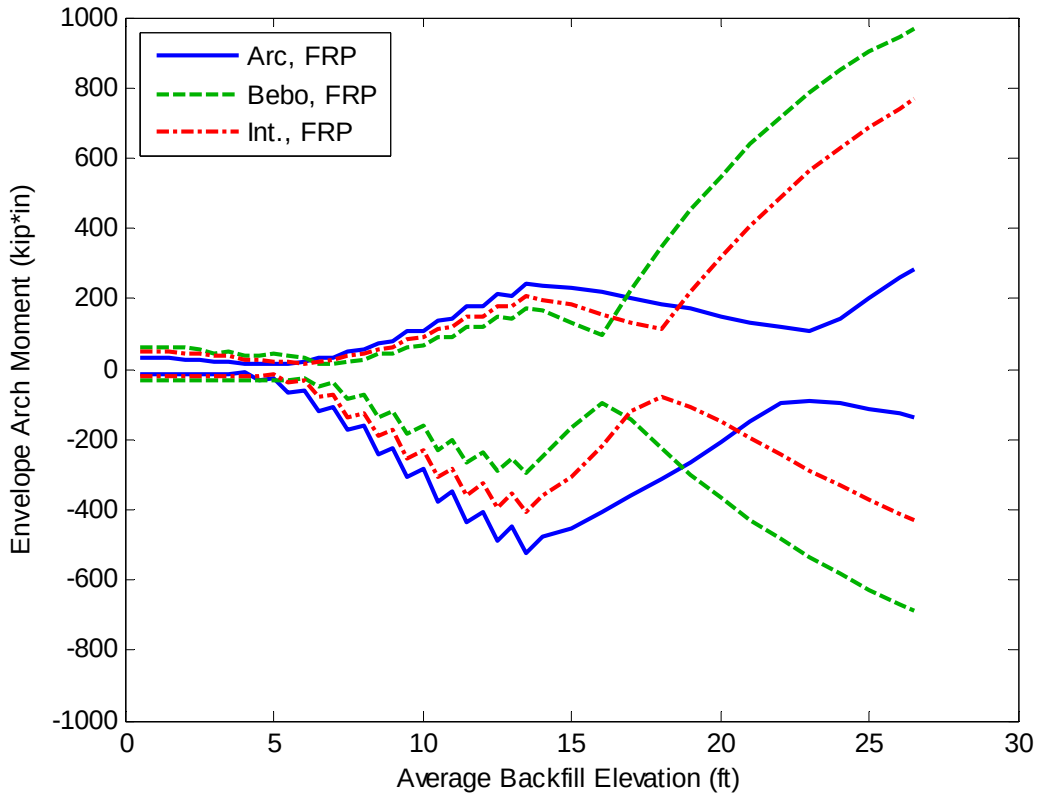

Figure 13 – Backfilling Envelope Arch Moments for Various Geometric Configurations, FRP Deck, 12.5 ft of Total Fill Above the Crown

It is apparent from Figure 12 and Figure 13 that the moment in the arch increases significantly at high backfill elevations going from the arc shape to the intermediate shape and again going from the intermediate shape to the Bebo shape. The reverse is true for the moment in the arch when the backfill elevation is near the height of the arch. This may indicate that shapes such as the Bebo arch are more appropriate for relatively small crown burial depths.

This test report shall not be reproduced, except in full, without the written approval of the AEWC Advanced Structures & Composites Center.

Outward Foundation Thrust

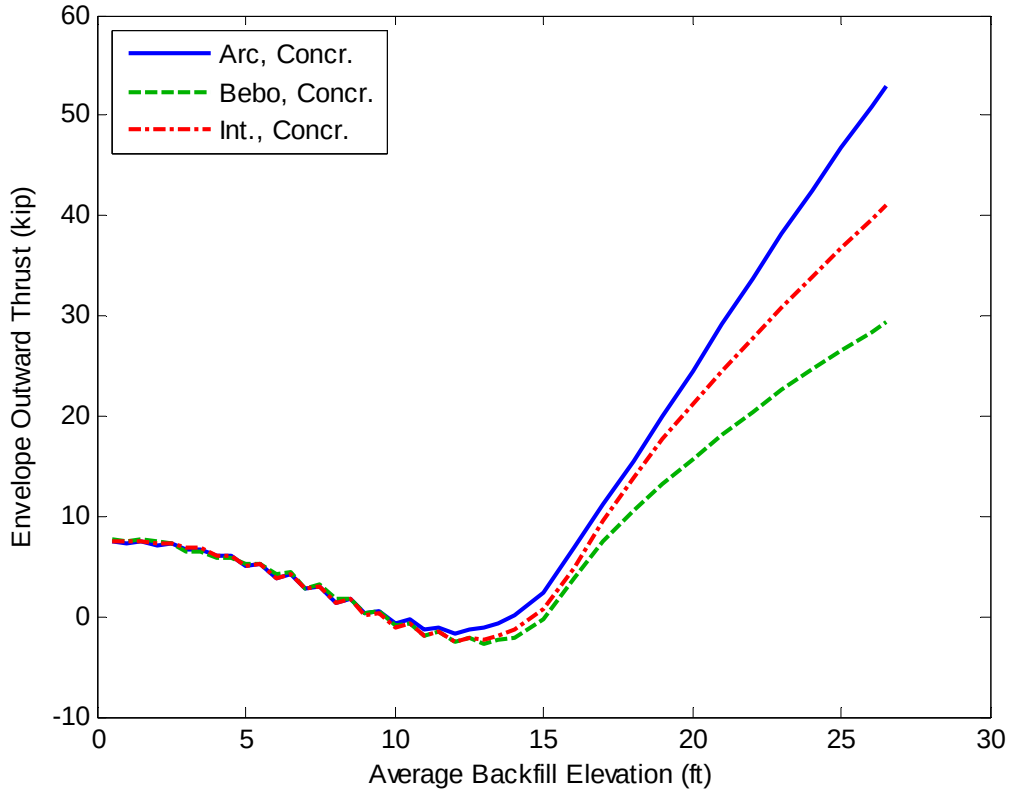

Figure 14 – Backfilling Envelope Outward Thrust for Various Geometric Configurations, Concrete Deck, 12.5 ft of Total Fill Above the Crown

This test report shall not be reproduced, except in full, without the written approval of the AEWC Advanced Structures & Composites Center.

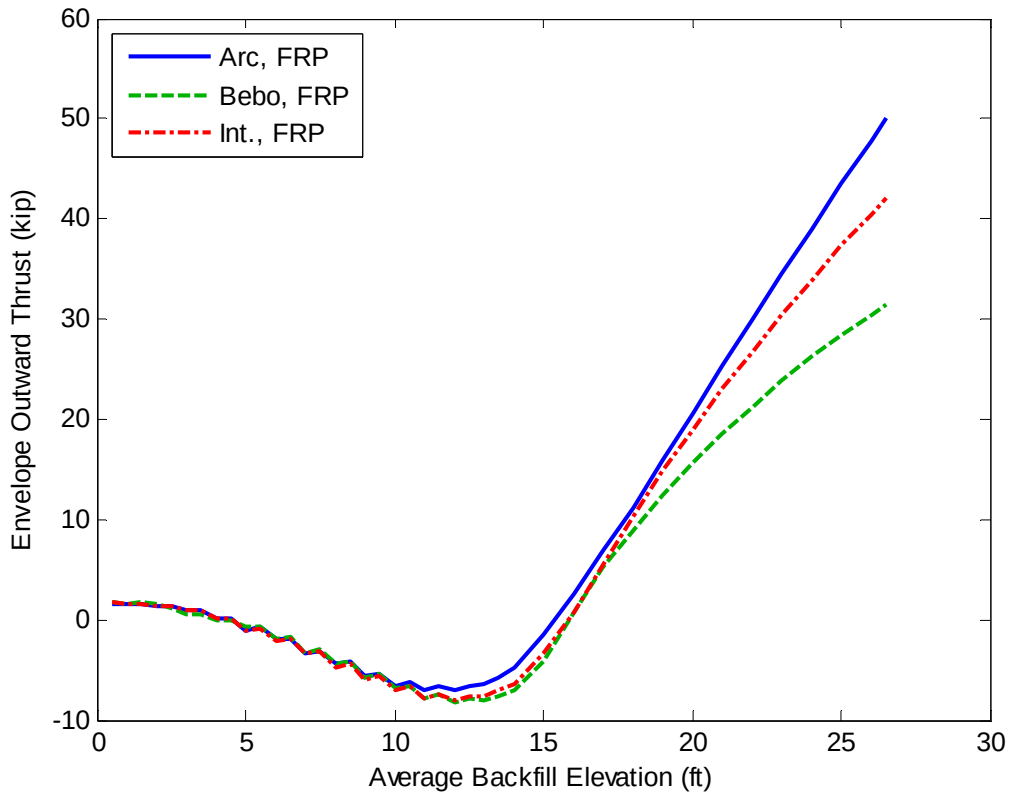

Figure 15 – Backfilling Envelope Outward Thrust for Various Geometric Configurations, FRP Deck, 12.5 ft of Total Fill Above the Crown

It is apparent from Figure 14 and Figure 15 that the outward thrust is generally greater for arc-shaped arches as compared to the Bebo arch for practically all levels of arch crown burial. Once again the response of the intermediate arch is in between the two others. This indicates that shapes that are relatively steeper near the supports and flatter near midspan are more effective at reducing foundation thrust loads.

This test report shall not be reproduced, except in full, without the written approval of the AEWC Advanced Structures & Composites Center.

Envelope Arch Axial Load

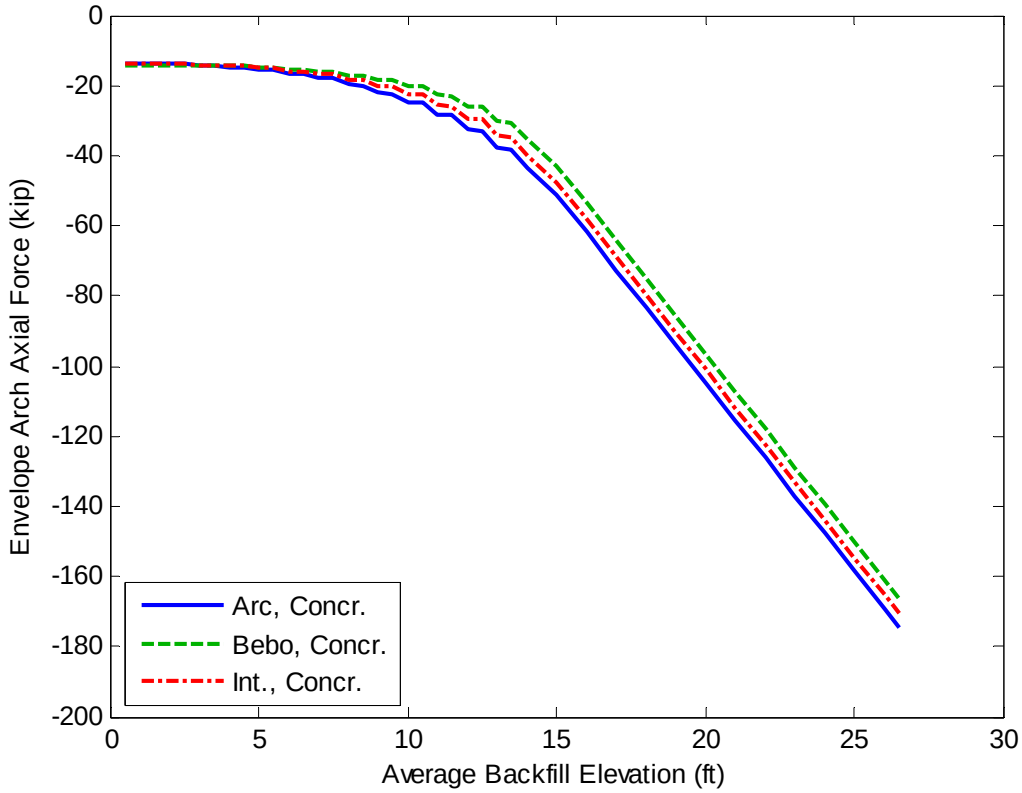

Figure 16 – Backfilling Envelope Arch Axial Load for Various Geometric Configurations, Concrete Deck, 12.5 ft of Total Fill above the Crown

This test report shall not be reproduced, except in full, without the written approval of the AEWC Advanced Structures & Composites Center.

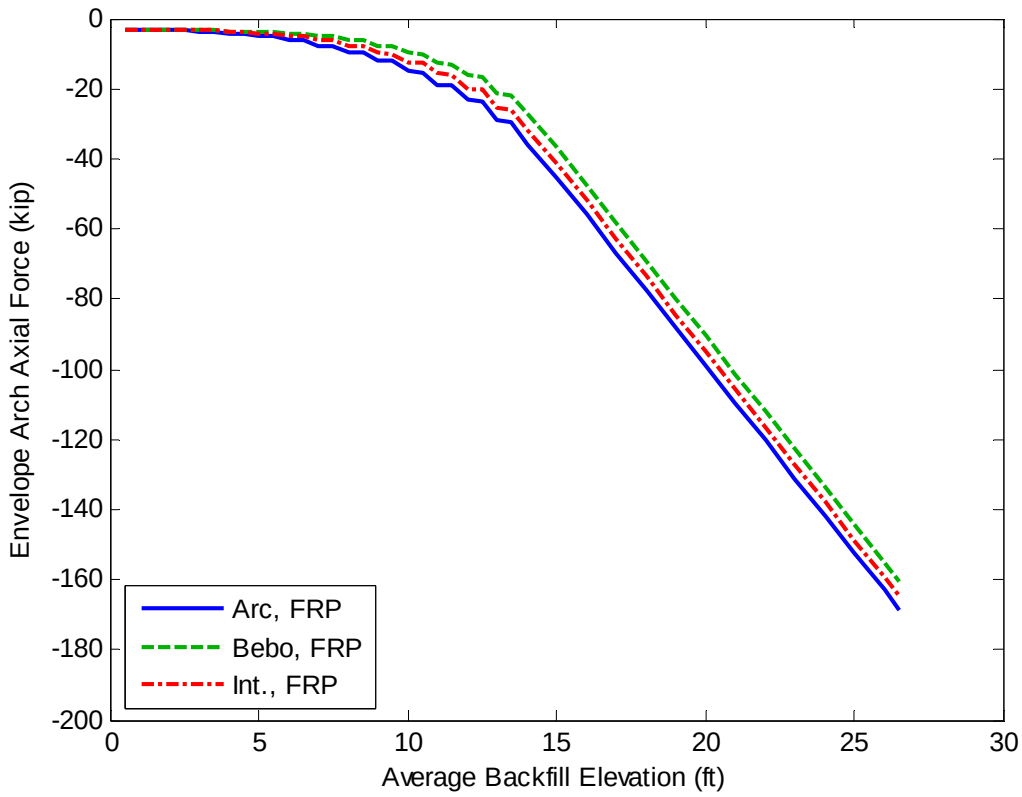

Figure 17 – Backfilling Envelope Arch Axial Load for Various Geometric Configurations, FRP Deck, 12.5 ft of Total Fill above the Crown

The maximum axial load level in the arch does not appear to be greatly affected by the shape of the arch based on Figure 16 and Figure 17, although the arc-shaped arch does carry slightly greater axial loads at all backfill levels.

Results: effect of live loading

The response due to live loading may control the design of the arch members, particularly for bridges with relatively low soil depth above the crown of the arch. The effect of soil-structure interaction on live loading was examined in this study by analyzing a variety of configurations as summarized in Table 4. Four different truck/position combinations provided by AIT were analyzed. The position refers to the front axle of the truck moving from left to right and the origin of the coordinate system is at midspan. Note that the positions referring to M+ in the right footing were actually applied with the truck

This test report shall not be reproduced, except in full, without the written approval of the AEWC Advanced Structures & Composites Center.

mirrored about midspan to maximize M+ in the left footing of the model. This was done because the positive moment is larger at the left footing due to staged backfilling. If staged backfilling were not considered, the foundation moments on each side of the arch due to construction would be equal. All analyses with live loading considered a final backfilling elevation of 15 ft (3 ft crown burial depth) unless otherwise noted. Service (unfactored) loads are used for all analyses.

Table 4 Matrix of Analyses to Examine the Effect of Arch Geometry

Truck and Position of Front Axle	**Maximizes**	**Arch Geometry**	**Decking**
Short Design Truck at 130 in (266 in Rev.)	M+ at right footing (M+ at left footing)	Circular Segment Arc	Concrete
Short Design Truck at 466 in	M- at right footing	ConSpan Bebo Arch	FRP-only
Tandem at -38 in (86 in Rev.)	M+ at right footing (M+ at left footing)	--	--
Tandem at 154 in	M- at right footing	--	--

This test report shall not be reproduced, except in full, without the written approval of the AEWC Advanced Structures & Composites Center.

Envelope Arch Moments

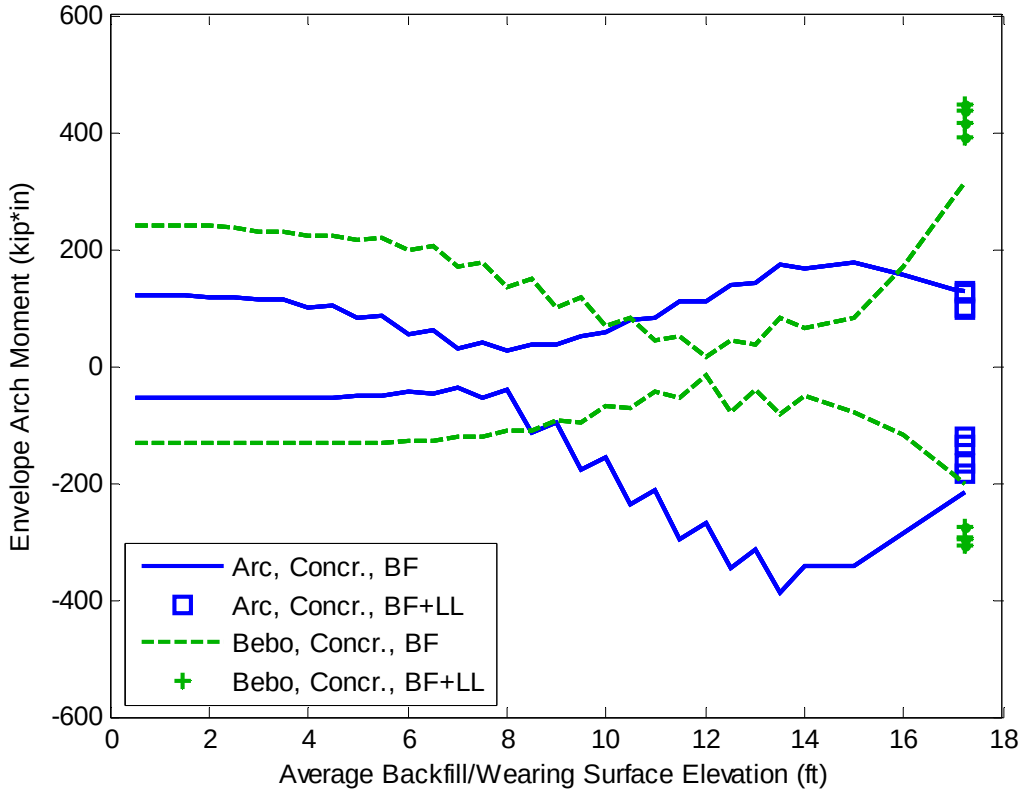

Figure 18 – Backfilling and LL Envelope Arch Moment for Arc and ConSpan (Bebo) Geometries (All 4 LL Analyses Shown for Each), Concrete Deck

This test report shall not be reproduced, except in full, without the written approval of the AEWC Advanced Structures & Composites Center.

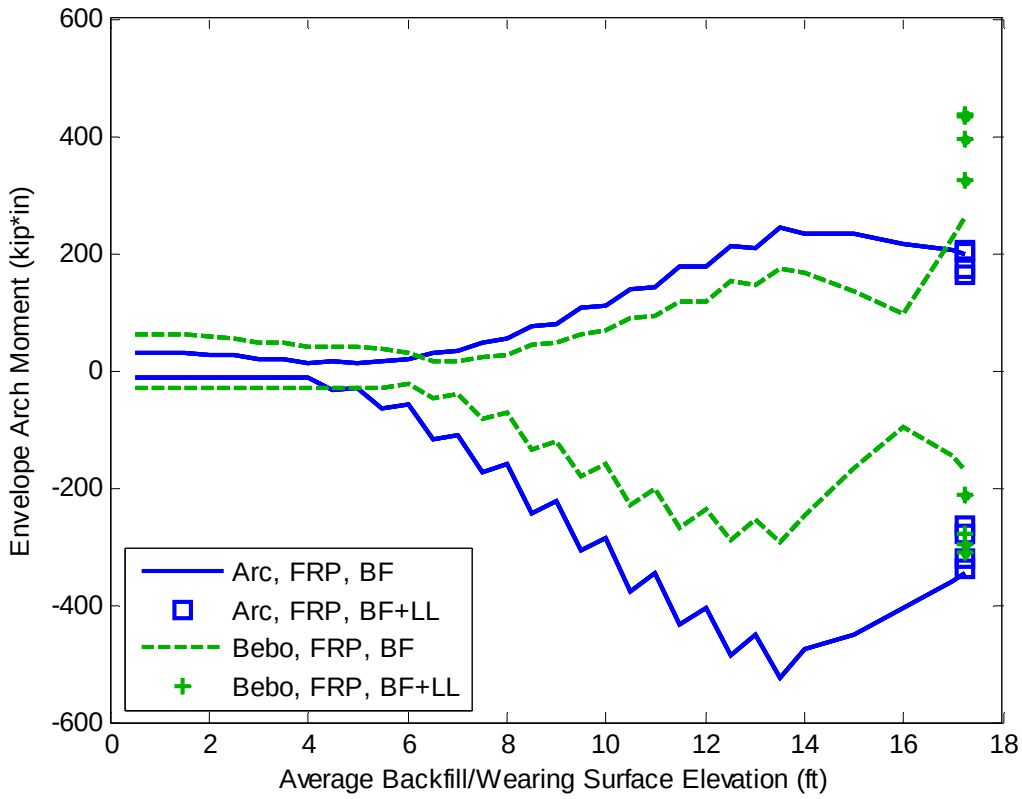

Figure 19 – Backfilling and LL Envelope Arch Moment for Arc and ConSpan (Bebo) Geometries (All 4 LL Analyses Shown for Each), FRP Deck

Interestingly, the magnitude of the arch moment due to live loading for the arc-shaped arches at all truck positions except one decreased as shown in Figure 18 and Figure 19. The one case that showed an increase in arch moment was only about 1%. This counter-intuitive result occurs because the crown burial depth is low (3 ft) and the arch is in such a position that it benefits from being "pushed back into place" by additional vertical loading (see Figure 7). On the other hand, the arch moment magnitudes increase for all possible scenarios with the Bebo arch. This indicates that the arc-shaped arch is more effective for resisting moment due to live loads at low crown burial depths.

This test report shall not be reproduced, except in full, without the written approval of the AEWC Advanced Structures & Composites Center.

Outward Foundation Thrust

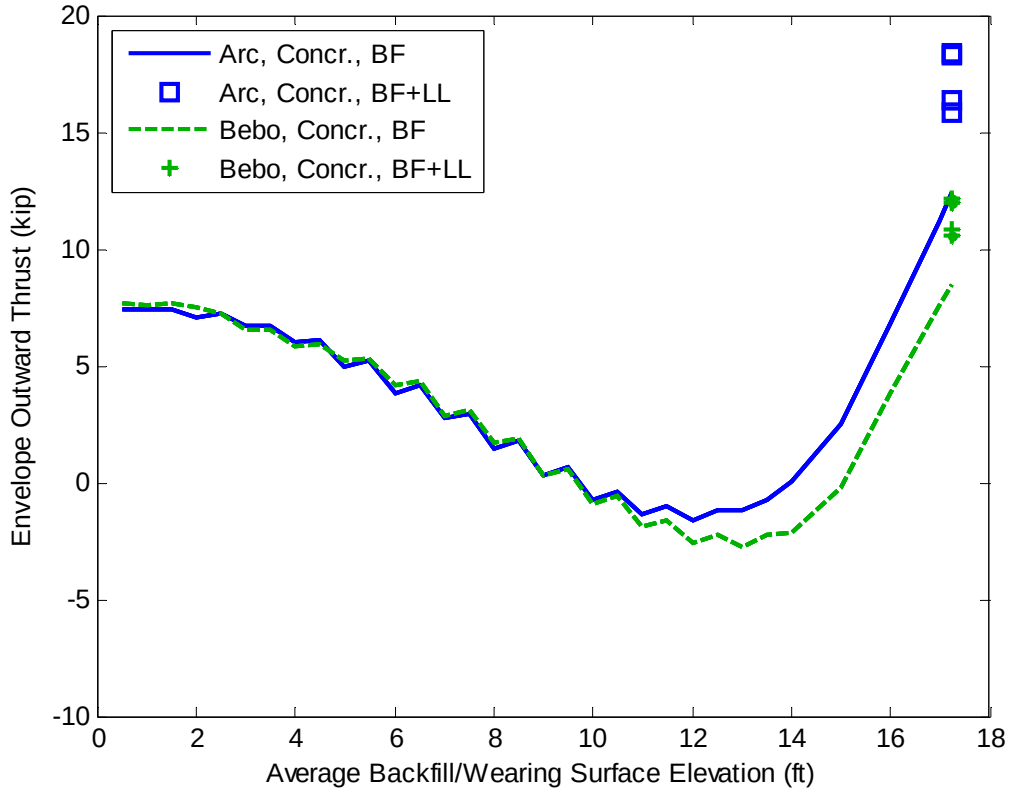

Figure 20 – Backfilling and LL Envelope Outward Thrust for Arc and ConSpan (Bebo) Geometries (All 4 LL Analyses Shown for Each), Concrete Deck

This test report shall not be reproduced, except in full, without the written approval of
the AEWC Advanced Structures & Composites Center.

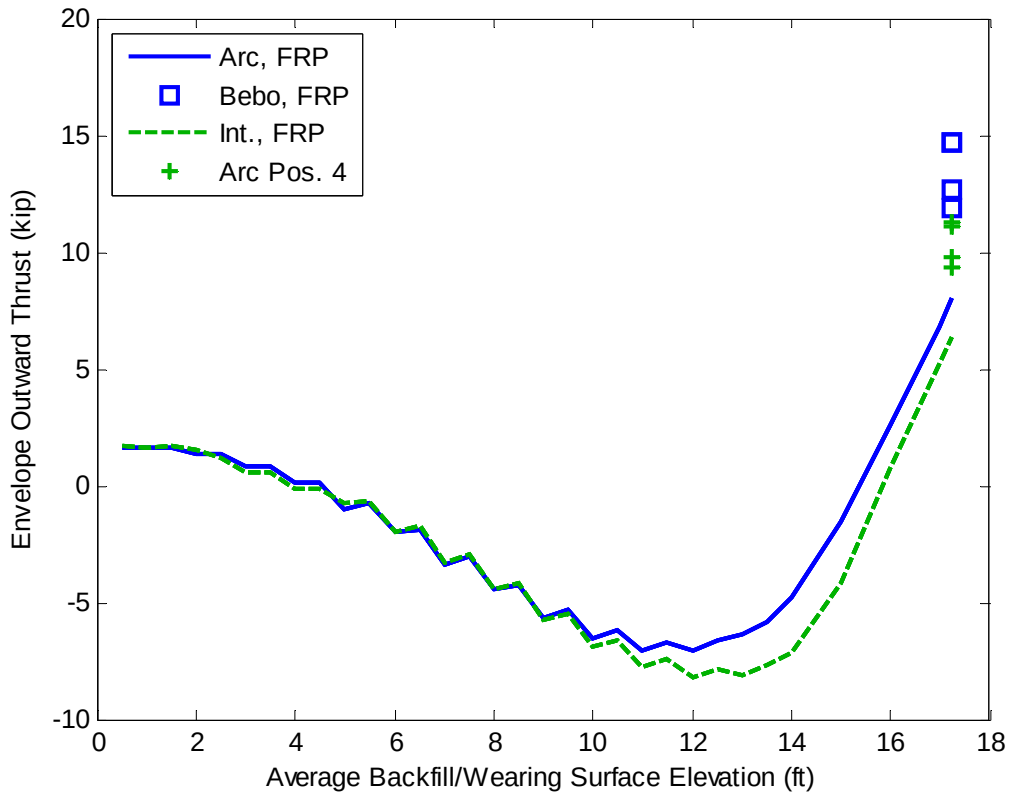

Figure 21 – Backfilling and LL Envelope Outward Thrust for Arc and ConSpan (Bebo) Geometries (All 4 LL Analyses Shown for Each), FRP Deck

It is apparent from Figure 20 and Figure 21 that the outward thrust is generally greater for arc-shaped arches as compared to the Bebo arch for practically all backfill and live load levels. This indicates that shapes that are relatively steeper near the supports and flatter near midspan are more effective at reducing foundation thrust loads due to backfilling and live loads.

This test report shall not be reproduced, except in full, without the written approval of
the AEWC Advanced Structures & Composites Center.

Envelope Arch Axial Load

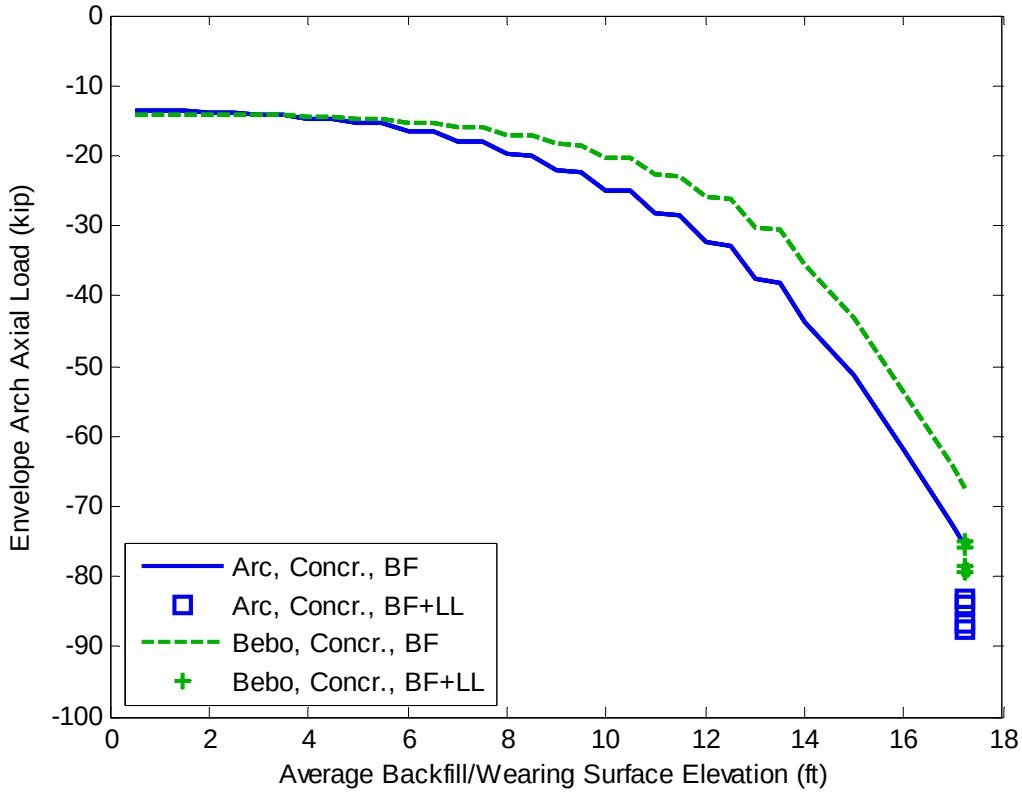

Figure 22 – Backfilling and LL Envelope Arch Axial Load for Arc and ConSpan (Bebo) Geometries (All 4 LL Analyses Shown for Each), Concrete Deck

This test report shall not be reproduced, except in full, without the written approval of
the AEWC Advanced Structures & Composites Center.

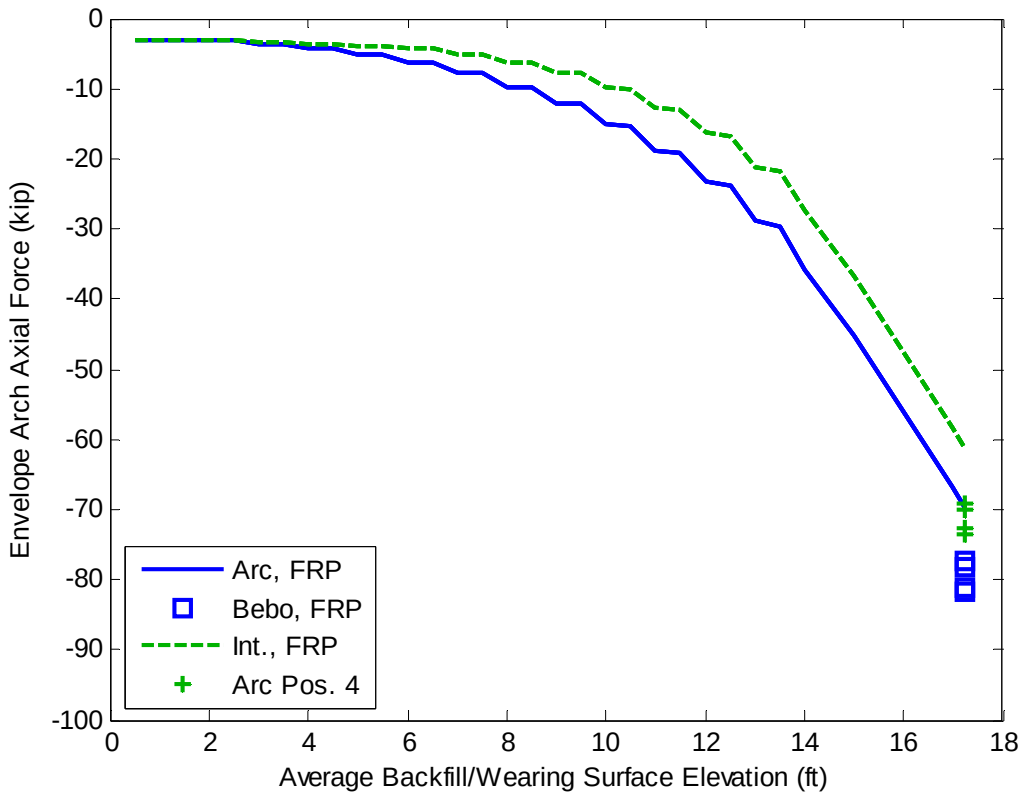

Figure 23 – Backfilling and LL Envelope Arch Axial Load for Arc and ConSpan (Bebo) Geometries (All 4 LL Analyses Shown for Each), FRP Deck

The change in axial load level in the arch due to live loading appears to be very similar for both arch shapes based on Figure 22 and Figure 23. Again the arc-shaped arch carries greater axial loads at all backfill levels.

Relative effect of soil springs

All analysis results presented to this point have utilized the procedure developed as part of this study with nonlinear soil springs. It is of interest to directly compare these results with those that would be generated with existing analysis code that does not consider nonlinear soil springs. A limited set of results is presented here to examine this.

This test report shall not be reproduced, except in full, without the written approval of the AEWC Advanced Structures & Composites Center.

Envelope Arch Moment

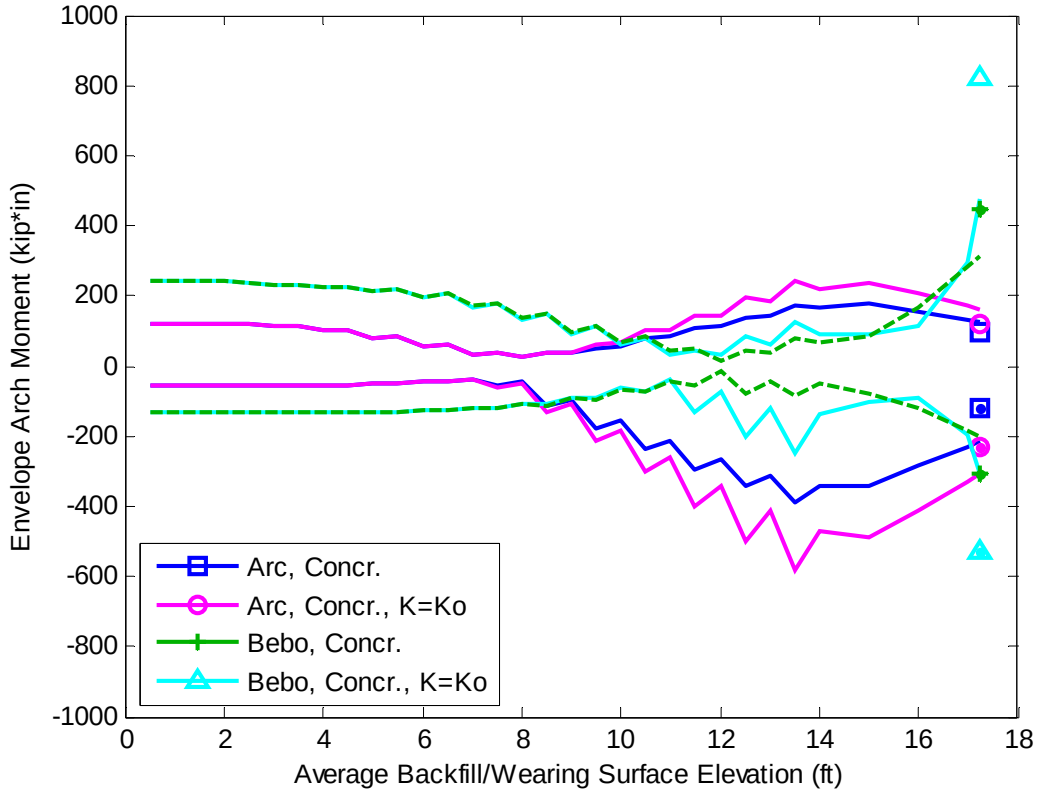

Figure 24 – Effect of Soil Springs on Backfilling and LL Moment, Concrete Deck, 3 ft of Backfill above the Crown

This test report shall not be reproduced, except in full, without the written approval of the AEWC Advanced Structures & Composites Center.

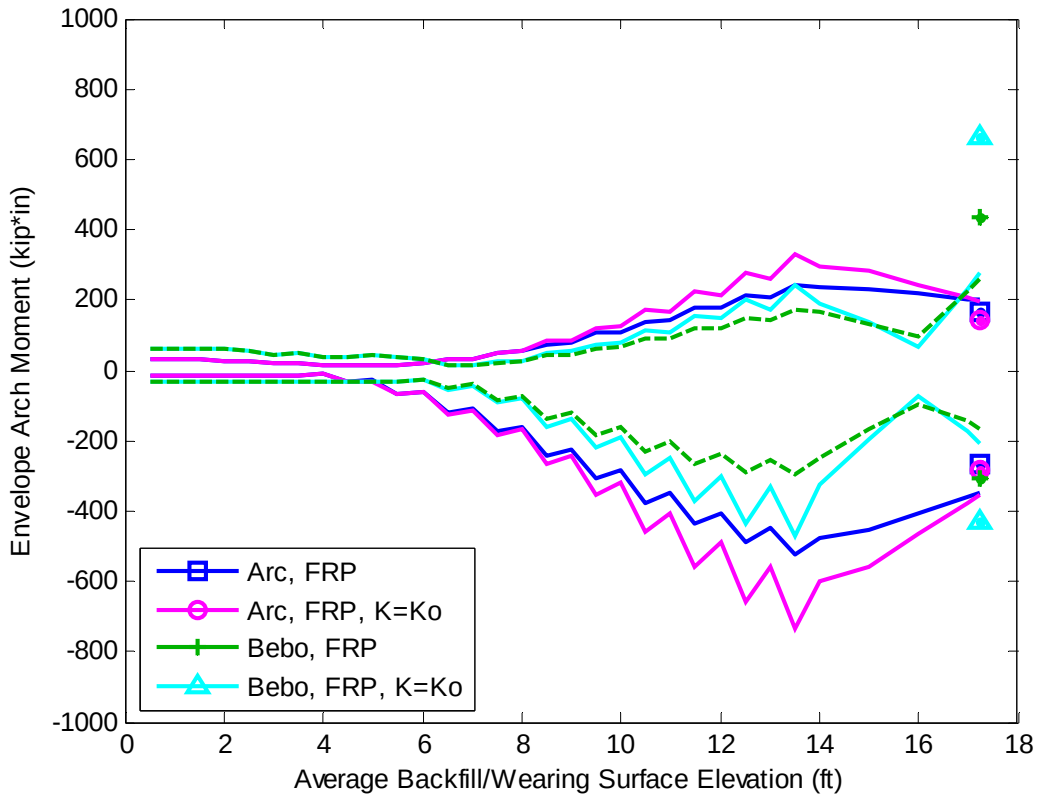

Figure 25 – Effect of Soil Springs on Backfilling and LL Moment, FRP Deck, 3 ft of Backfill above the Crown

It is apparent from Figure 24 and Figure 25 that the arch bending moment in both the arc-shaped arch and the Bebo arch are significantly reduced by considering the nonlinear soil spring relationship. The peak bending moment magnitudes and relative difference between the two types of arches are presented in Table 5. For all scenarios presented, the nonlinear soil spring relationship results in a reduction in arch bending moment of 26-46%.

Table 5 Peak Moment Magnitudes and Relative Differences Due to the Consideration of Nonlinear Soil Springs, 3 ft of Backfill above the Crown

		Arc			**Bebo**		
Deck	**Param**	**Nonlinear**	**K = Ko**	**Diff.**	**Nonlinear**	**K = Ko**	**Diff.**
Concr.	M+ (kip*in)	176	244	28%	447	823	46%
	M- (kip*in)	-386	-583	34%	-306	-532	42%

This test report shall not be reproduced, except in full, without the written approval of the AEWC Advanced Structures & Composites Center.

FRP	M+ (kip*in)	243	328	26%	436	666	35%
	M- (kip*in)	-523	-736	29%	-309	-470	34%

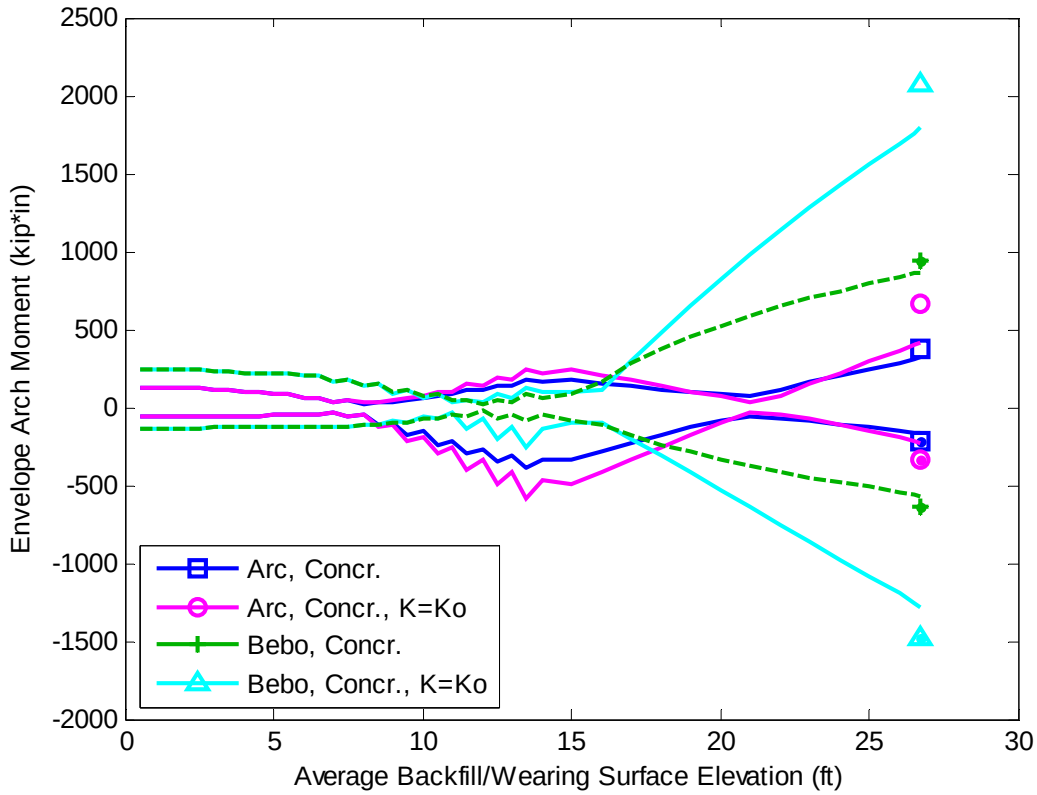

Figure 26 – Effect of Soil Springs on Backfilling and LL Moment, Concrete Deck, 12.5 ft of Backfill above the Crown

This test report shall not be reproduced, except in full, without the written approval of the AEWC Advanced Structures & Composites Center.

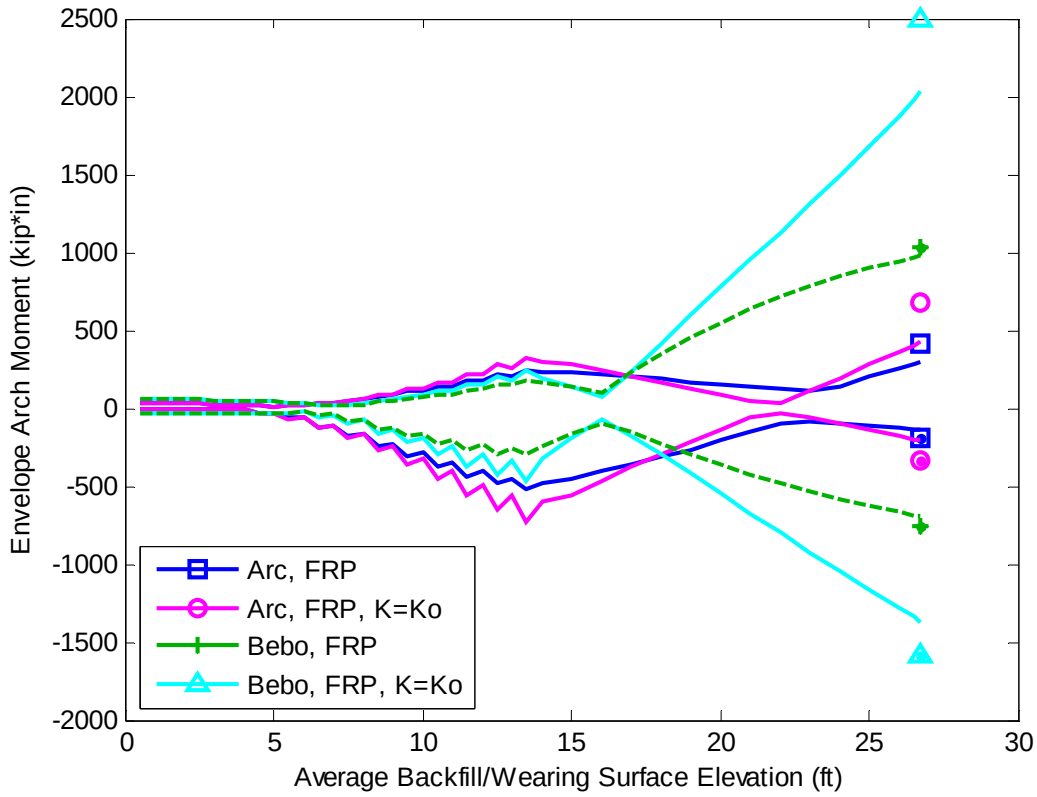

Figure 27 – Effect of Soil Springs on Backfilling and LL Moment, FRP Deck, 12.5 ft of Backfill above the Crown

It is apparent from Figure 26 and Figure 27 that the arch bending moment in both the arc-shaped arch and the Bebo arch are significantly reduced by considering the nonlinear soil spring relationship. The peak bending moment magnitudes and relative difference between the two types of arches are presented in Table 6. For all scenarios presented, the nonlinear soil spring relationship results in a reduction in arch bending moment of 37-59%.

Table 6 Peak Moment Magnitudes and Relative Differences Due to the Consideration of Nonlinear Soil Springs, 12.5 ft of Backfill above the Crown

		Arc			**Bebo**		
Deck	**Param**	**Nonlinear**	**K = Ko**	**Diff.**	**Nonlinear**	**K = Ko**	**Diff.**
Concr.	M+ (kip*in)	379	664	43%	935	273	55%
	M- (kip*in)	-212	-334	37%	-633	-1481	57%

This test report shall not be reproduced, except in full, without the written approval of the AEWC Advanced Structures & Composites Center.

FRP	M+ (kip*in)	417	674	38%	1032	2500	59%
	M- (kip*in)	-196	-340	42%	-762	--1581	52%

This test report shall not be reproduced, except in full, without the written approval of
the AEWC Advanced Structures & Composites Center.

Envelope Outward Thrust

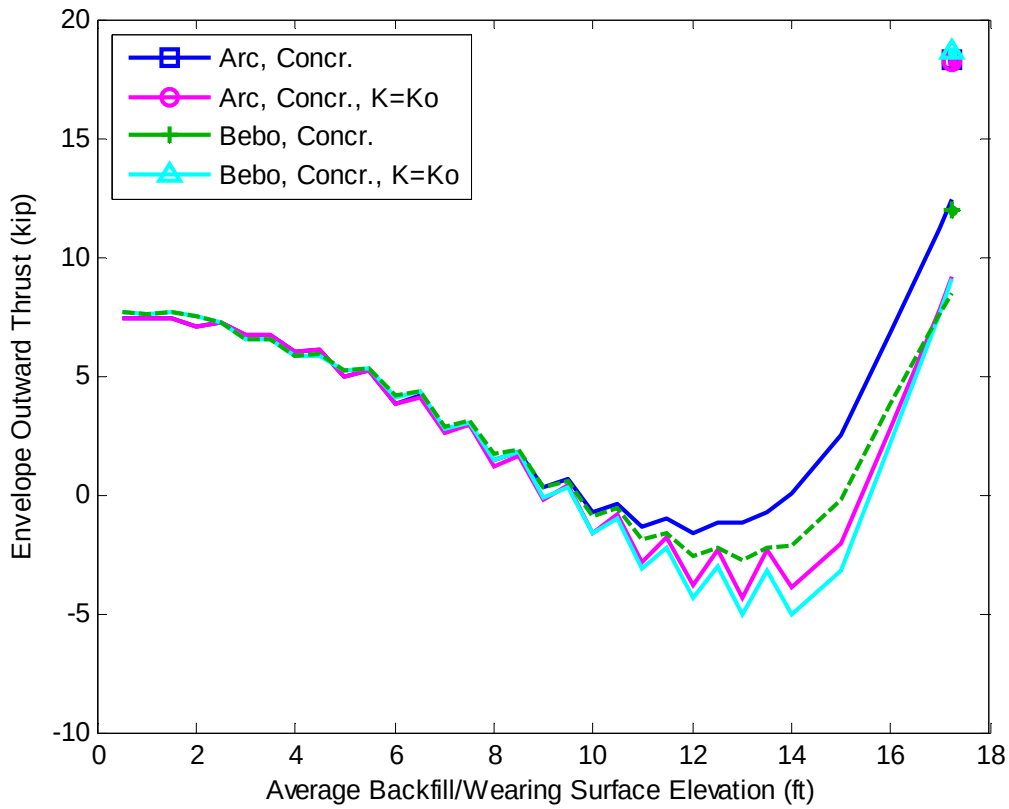

Figure 28 – Effect of Soil Springs on Backfilling and LL Thrust, Concrete Deck, 3 ft of Backfill above the Crown

This test report shall not be reproduced, except in full, without the written approval of the AEWC Advanced Structures & Composites Center.

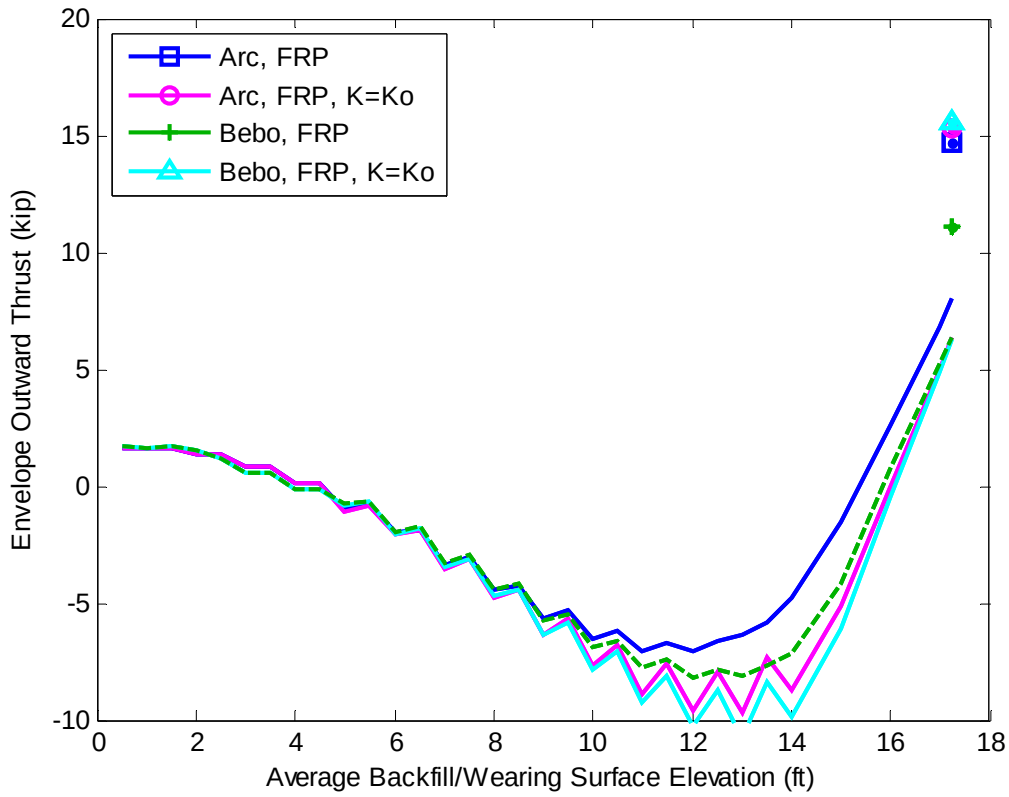

Figure 29 – Effect of Soil Springs on Backfilling and LL Thrust, FRP Deck, 3 ft of Backfill above the Crown

The outward thrust magnitude is reduced 29-36% when considering a nonlinear soil spring relationship for the Bebo arch, but it has practically no effect on the arc-shaped arch as shown in Table 7. The reason for the lack of significant benefit with respect to outward thrust with the arc-shaped arch is that many of the soil springs are actually still in the active state (i.e. K < Ko) at a backfill depth of the 3 ft. After the application of live loads, which causes K to increase, the response is similar to that for linear soil springs (K = Ko). As shown next, the soil-springs are more effective for larger crown burial depths.

Table 7 Peak Outward Thrust Magnitudes and Relative Differences Due to the Consideration of Nonlinear Soil Springs, 3 ft of Backfill above the Crown

		Arc			**Bebo**		
Deck	**Param**	**Nonlinear**	**K = Ko**	**Diff.**	**Nonlinear**	**K = Ko**	**Diff.**

This test report shall not be reproduced, except in full, without the written approval of the AEWC Advanced Structures & Composites Center.

Concr.	Outward Thrust	18.3	18.2	-1%	11.9	18.7	36%
FRP	Outward Thrust	14.7	15.3	4%	11.1	15.6	29%

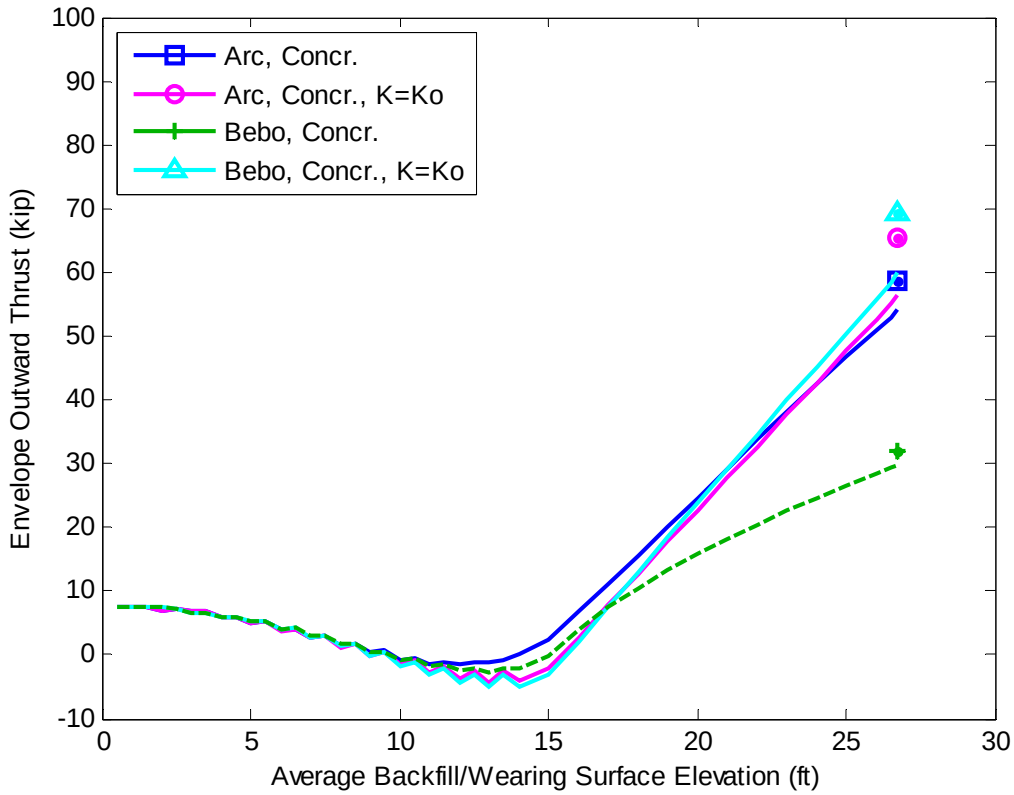

Figure 30 – Effect of Soil Springs on Backfilling and LL Thrust, Concrete Deck, 12.5 ft of Backfill above the Crown

This test report shall not be reproduced, except in full, without the written approval of the AEWC Advanced Structures & Composites Center.

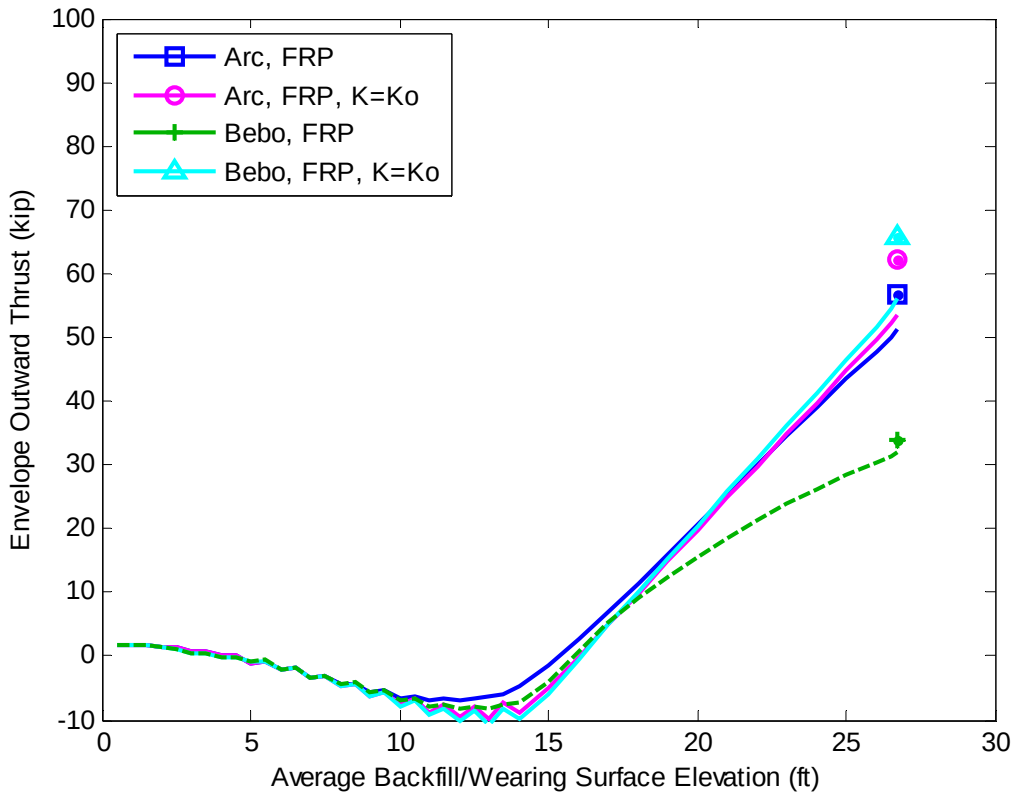

Figure 31 – Effect of Soil Springs on Backfilling and LL Thrust, FRP Deck, 12.5 ft of Backfill above the Crown

The outward thrust magnitude is reduced 48-54% when considering a nonlinear soil spring relationship for the Bebo arch, but only 8-10% for the arc-shaped arch as shown in Table 8 for a crown burial depth of 12.5 ft. This indicates that the use of nonlinear soil springs provides more benefit for the Bebo arch than the arc-shaped arch with respect to the improvement in foundation thrust. Additional improvement may be mobilized for both shapes when other types of foundations are considered (e.g. spread footings free to translate instead of the perfectly fixed foundations that are assumed in these analyses).

Table 8 Peak Outward Thrust Magnitudes and Relative Differences Due to the Consideration of Nonlinear Soil Springs, 12.5 ft of Backfill above the Crown

		Arc			**Bebo**		
Deck	**Param**	**Nonlinear**	**K = Ko**	**Diff.**	**Nonlinear**	**K = Ko**	**Diff.**
Concr.	Outward Thrust	58.8	65.4	10%	69.3	31.9	54%

This test report shall not be reproduced, except in full, without the written approval of the AEWC Advanced Structures & Composites Center.

FRP	Outward Thrust	56.9	62.3	8%	65.8	33.9	48%

Envelope Arch Axial Load

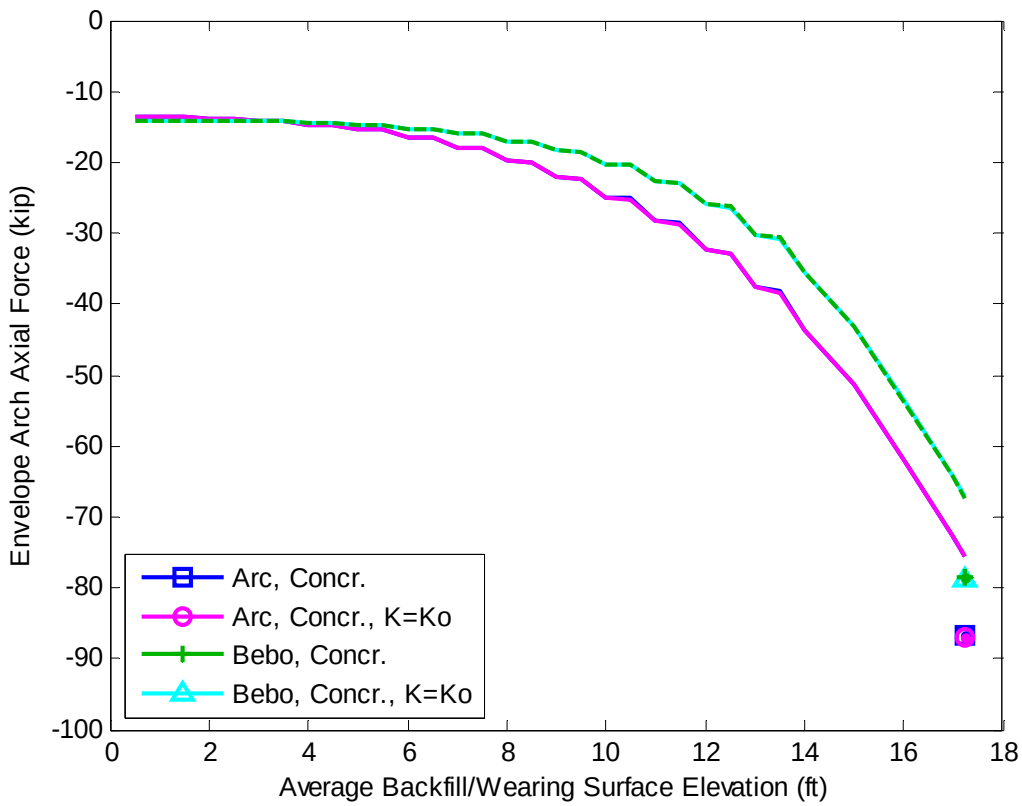

Figure 32 – Effect of Soil Springs on Backfilling and LL Arch Axial Loads, Concrete Deck, 3 ft of Backfill above the Crown

This test report shall not be reproduced, except in full, without the written approval of the AEWC Advanced Structures & Composites Center.

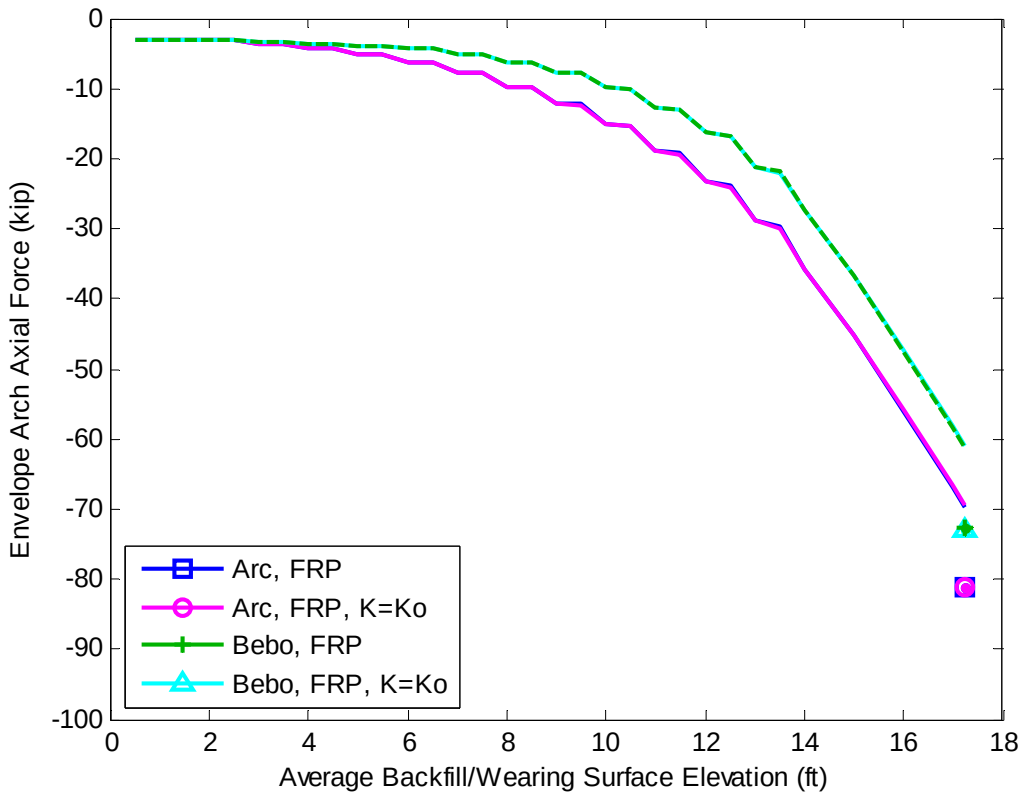

Figure 33 – Effect of Soil Springs on Backfilling and LL Arch Axial Loads, FRP Deck, 3 ft of Backfill above the Crown

The peak magnitude of arch axial force is practically unaffected by the soil spring relationship as shown in Figure 32, Figure 33, and Table 9. The difference in response is less than 1%.

Table 9 Peak Arch Axial Force Magnitudes and Relative Differences Due to the Consideration of Nonlinear Soil Springs, 3 ft of Backfill above the Crown

		Arc			**Bebo**		
Deck	**Param**	**Nonlinear**	**K = Ko**	**Diff.**	**Nonlinear**	**K = Ko**	**Diff.**
Concr.	Arch Axial Force (kip)	-78.6	-78.9	0.4%	-86.8	-87.1	0.3%
FRP	Arch Axial Force (kip)	-72.7	-72.9	0.3%	-81	-81.1	0.1%

This test report shall not be reproduced, except in full, without the written approval of the AEWC Advanced Structures & Composites Center.

AEWC Advanced Structures & Composites Center
5793 AEWC Bldg
University of Maine
Orono, ME 04469-5793

CONFIDENTIAL

Telephone: 207-581-2123
FAX: 207-581-2074
contactaewc@umit.maine.edu
www.aewc.umaine.edu

This test report shall not be reproduced, except in full, without the written approval of
the AEWC Advanced Structures & Composites Center.

Summary and conclusions

MATLAB-based structural analysis code has been developed to capture the effects of nonlinear soil springs, staged construction, decking stiffness, and longitudinal benefit from concrete decking. The effect of staged backfilling, arch geometry, and live loading was investigated by analyzing a variety of configurations that are representative of a proposed (or previously constructed) bridge project. Input parameters were based on values provided by AIT and were primarily based on the proposed Ellsworth Bridge project.

The following conclusions were drawn from results of analyses:

Staged Backfilling

1. Alternating soil lifts resulted in side-sway and non-symmetric response about midspan.
2. Staged backfilling allowed lateral earth pressure coefficients other than the at-rest coefficient to be rationally considered.
3. Staged backfilling allowed the structural response to be tracked throughout the construction period.
4. The bending moment response for the arch with the nonlinear bending stiffness relationship generally fell between those for the linear cracked arch and the linear uncracked arch.
5. The maximum moment during backfilling sometimes occurred at a point prior to the last construction load step depending on the total backfill level.
6. The type of arch bending stiffness considered did not have a large effect on the outward thrust.
7. The outward thrust was initially larger for the concrete-decked arches compared to the FRP-decked arches due to the increased self-weight.
8. The type of arch bending stiffness had practically no effect on the maximum axial load in the arch.

Arch Geometry

1. The shape of the arch had a large effect on the moment developed within the arch (total span and rise were held constant). Shapes that were steeper near supports and flatter near midspan (Bebo) resulted in much larger bending moments at large burial depths.

This test report shall not be reproduced, except in full, without the written approval of the AEWC Advanced Structures & Composites Center.

2. At shallow burial depths, the moments were largest in the arc-shaped arch and least for the Bebo arch, which may indicate that the optimal shape is dependent on crown burial depth.
3. The outward foundation thrust was greatest for the arc-shaped arch and least for the Bebo arch at all levels of backfilling.
4. The axial load in the arch was minimally affected by the arch shape, although the axial load in the Bebo arch was smaller for all levels of backfilling.

Live Loading

1. The magnitude of moment in the arc-shaped arch decreased as live loads were applied. This counter-intuitive result occurs when the crown burial depth is low (3 ft) and the arch is in such a position that it benefits from being "pushed back into place" by additional vertical loading (see Figure 7).
2. The magnitude of moment in the Bebo arch increased as live loads were applied, which may indicate that the arc-shaped arch is more effective for resisting moment due to live load at low crown burial depths.
3. The outward thrust due to live loading is greater for arc-shaped arches than the Bebo arch.
4. The change in axial load level due to live loading was similar for both arches. The total axial loads were larger in the arc-shaped arch compared to the Bebo arch.

Relative Effect of Soil Springs

1. The use of nonlinear soil springs resulted in 26-59% lower arch bending moments.
2. Outward thrust was reduced by 29-54% for the Bebo arch. Less significant differences of around 0-10% were noted for the arc-shaped arch. It is expected that the relative effect of the soil-springs with respect to outward thrust will be reduced further for arches with other types of foundations that allow lateral movements (e.g. spread footings or pile-supported foundations).
3. The soil springs had practically no effect on the axial load level in the arches.

In summary, the consideration of nonlinear soil springs, the 3D effect of transverse decking stiffness, staged backfilling, and various arch geometries was shown to have a significant effect on the critical response values that would be used to design bridge structures. Many of the critical response values were reduced significantly by considering

This test report shall not be reproduced, except in full, without the written approval of
the AEWC Advanced Structures & Composites Center.

nonlinear soil springs. It was also shown that the arch geometry had a large effect on critical response values. The software developed as part of this project will provide a valuable tool to bridge designers in their efforts to optimize designs to achieve desired effects and ultimately improve the economic efficiency of these structures.

This test report shall not be reproduced, except in full, without the written approval of
the AEWC Advanced Structures & Composites Center.

Task 2.2 Improved decking design

Efficient design of this bridge system needs to incorporate a greater spacing of the arches. The largest barrier to this has been the inability of the FRP decking product to span between the arches and carry the loads through the soil to the arches. At this time a new decking design was investigated to improve on the Enduro Composites Tuff Span decking as well as the cast-in-place (CIP) concrete deck used on all the bridges to date. This stronger decking material allows for a greater spacing of the carbon fiber reinforced arches. Increasing the spacing of the arches decreases cost and could potentially eliminate the concrete overlay presently used. Additionally, using structural CIP concrete is time consuming and expensive because of the rebar placement and cure time required. This work aimed at identifying commercial products that would allow arches to be spaced up to 6 feet on center with anticipated future geometries and at-rest soil pressures. This new decking product would also be much more durable and be expected to withstand significant damage without compromising the integrity of the structure.

Several panel products with the capacity to span between the arches were identified. Only one product found was to be able to conform to an arch shape. The products investigated include DuraSpan by Martin Marietta Composites, ZellComp FRP bridge decks, Superdeck by Creative Pultrusions, and SuperRail by Creative Pultruions. All of the products are rigid wide flat panels that are intended for typical girder systems except for SuperRail. DuraSpan is a commercially available bridge deck system in use as a direct replacement for concrete decks over steel girders. ZellComp FRP bridge decks are similar. Images of these two products can be seen in Figure 34 and Figure 35.

This test report shall not be reproduced, except in full, without the written approval of
the AEWC Advanced Structures & Composites Center.

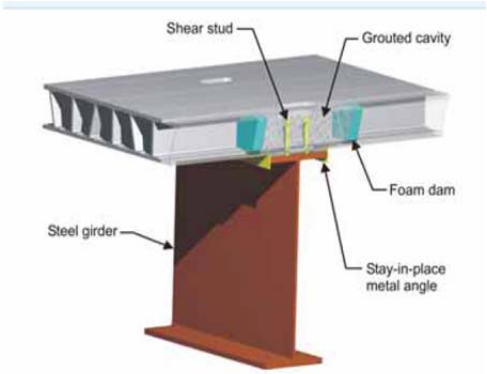

Figure 34 – DuraSpan Cross-section

Figure 35 – ZellComp During Construction

Other composite roofing deck products similar to the Enduro Composites, TuffSpan roof deck product were also investigated. There are several products available but do not have the strength to span between the arches with the soil pressures anticipated for these structures. These other products include corrugated composite roof panels such as Suntuf and Palruf. They are available commercially but are weak and intended for only minor spans and light loading.

Panels that could conform to an arch shape were analyzed as beam elements with a unit width. Simplified, conservative loads were used in the Neal Bridge analysis. This analysis found a maximum total service soil pressure of 1725 psf (Goslin 2009). This value was used for analysis of panels in initial screening calculations.

A product was identified that met the goals previously described. The SuperRail Composite Guardrail is manufactured and sold by Creative Pultrusions, Inc. and has been approved by FHWA as a guardrail system (Baxter 2003). Two components were included in the evaluating the feasibility of this decking system: 1) structural analysis of this system under the uniform soil and bearing loads and 2) determination of whether this panel will conform to the arch shape of the FRP tubular members.

Creative Pultrusions provided calculations that included predicted deflections and a 3D finite element analysis on their product in an arrangement similar to the Ellsworth bridge to be replaced in 2011 with the Bridge-in-a-Backpack™. The analysis was conducted to evaluate the product for its feasibility in use as part of the bridge system. Loads were provided by AIT. The analysis showed a soil pressure of roughly 49.3 psi at ultimate failure of the decking. The failure mode at this load was web buckling at the bearing of

This test report shall not be reproduced, except in full, without the written approval of
the AEWC Advanced Structures & Composites Center.

each panel assuming there is no stiffener or panel overlap at this location, which is shown in Figure 36.

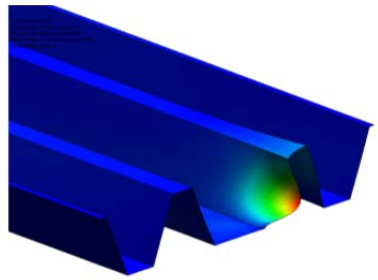

Figure 36 – Deformed shape of panel at failure from FE analysis (courtesy of Creative Pultrusions, Inc.)

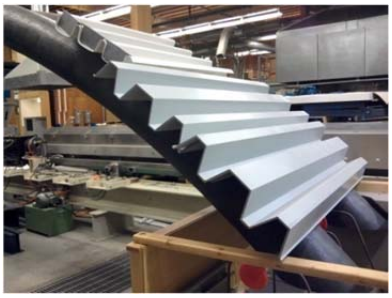

Figure 37 - Mock up of Composite Decking

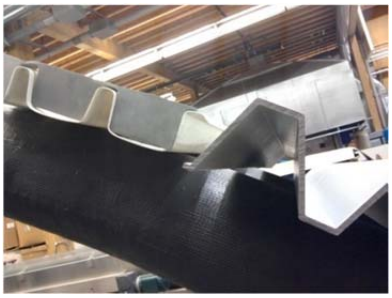

Figure 38 - Elevation of "New" & "Old" Decking

A section of the decking on a mock up in the lab can be seen in Figure 37 and Figure 38. A mockup of a bridge section was completed to evaluate whether the decking would conform to an arch shape, and could be installed successfully. This product conformed relatively well. It is very rigid in the weak axis of the panel but is narrow enough that for most radii of curvature the straight panel sections can be attached and conformed to the arch shape. Tuff Span and SuperRail properties are shown in Table 10 with a factor of safety of 2.5 for comparisons and analyzed for a typical buried arch section with a 24” cover at the crown. Deep sections were ignored where higher soil loads control.

This test report shall not be reproduced, except in full, without the written approval of the AEWC Advanced Structures & Composites Center.

Table 10 – Summary of Panel Products

Product	Moment Capacity (kip-in/ft)	Bearing Capacity (kip/ft)	Achievable Span (ft-in)	Conforms Easily to Arch Shape
Tuff Span (Bannon 2009)	12.4	2.1	3'-0"	Yes
SuperRail (Mostoller 2011)	114.4	34.0	6'-0" +	Yes
PalRuf/SunTuf	Negligible	Negligible	Negligible	Yes
DuraSpan	Not available	Not available	10'-0"	No
Superdeck (Creative Pultrusion 2011)	314	32	9'-0"	No
ZellComp (Richards 2011)	384	38	Not available	No

The strength and stiffness of this panel in the transverse direction of the bridge (longitudinal and strong axis of the panel) can be compared to the Tuff Span 8.0 Series 700 panel in the same direction. The stiffness of the CP-155 panel, EI, in the panel longitudinal direction is conservatively 82,160 kip-in^2 and the Tuff Span panel is published to be 5,850 kip-in^2(Enduro Composites 2009). The flexural compressive strength of the CP-155 in the direction of the deck span is reported to be 68 ksi (Mostoller 2011). The flexural strength of the Tuff Span 8.0 Series 700 panel is published as 55 ksi.

The Creative Pultrusions FRP decking product meets the need of stronger and thicker FRP product to span between the arches and conform to an arch shape. This eliminates the large expense of designing a custom FRP shape and tooling. This product will allow for the elimination of a concrete deck with the addition of a waterproofing solution at the seams of the panels. AEWC will continue to look for products that fit this need as new products are introduced to the market, but at this time CP-155 is the best product available for this use.

Task 2.3 Advanced modeling tools

Compression of Hollow FRP

The rigidified carbon fiber arch system relies on concrete for compression capacity and shape stability. The system was designed as a cast in place concrete application with the arch structure serving as formwork. While serving this function, the concrete adds no

This test report shall not be reproduced, except in full, without the written approval of
the AEWC Advanced Structures & Composites Center.

capacity to the arch and the shell must carry construction loads – including wet concrete, workers, decking, and any equipment – until the concrete has cured. While the construction loads are much lower than the long term loads on the arch, the hollow strength and out of plane stiffness are much lower than that of the concrete-filled arch and local buckling of the shell wall during filling may be more critical than long term strength for some arch geometries.

According to Seide and Weingarten (1961), the short-column compression and bending capacities of a hollow shell are equivalent because both failures are controlled by local buckling of the compression face. Local and global buckling are irrecoverable deformations; local buckling is a change in cross sectional shape while global buckling is a change in member or structure orientation. Due to the high in-plane stiffness of an arch and the decking, which limits global out-of-plane deformations of the arches during concrete filling, global buckling is generally not a concern. However, due to the small thickness of the arch wall and the presence of a filling hole, local buckling failures are of concern for a full-scale hollow arch during concrete filling. Local buckling failures are not dependent on specimen length, provided the length is above crushing dominated failure and below Euler buckling failure, for pure axially loaded specimens. A short column in axial compression is considered to have – for the same material properties – the same compression face strength as a full sized arch. As short columns were easier to fabricate and test, short columns were tested in place of long arches or tubes for the majority of specimens.

Several models exist that give a predicted failure stress for local buckling of hollow sections in compression or bending (Timoshenko, 1935 Brazier, 1927 Donnell, 1934 and Kedward, 1978). All of these models are addressed by Kedward (1978). With the increased use of composites, buckling of composite cylinders has become a topic of interest for researchers. Hollow composites are not commonly used in highway infrastructure applications, but they are used in applications demanding a high strength to weight ratio, such as aerospace. An important subset currently being researched is anisotropic shells, shells with different fiber angles for different lamina. In these shells, buckling behavior is modified because the coupled flexure/torsion and potentially flexure/elongation and torsion/elongation can lead to early torsional buckling modes (Shen, 2008). If a cylinder made from a laminate schedule designed to maximize torsional buckling effect is compared in finite element modeling to a cylinder designed to minimize torsional buckling effect, the maximized model can have up to a 30% decrease capacity, despite having identical predicted capacity from classical buckling theory (Weaver, 2002).

Available analytical models exist for idealized homogeneous sections. The irregularity of the braid, native manufacturing defects (such as unintended curvature, diameter variation,

This test report shall not be reproduced, except in full, without the written approval of
the AEWC Advanced Structures & Composites Center.

and non-circular cross section) and material anisotropy produce out of plane eccentricities that reduce the compressive buckling capacity of the thin wall composite tubes considered in this study. Therefore, laboratory tests have been performed on a variety of cross sectional geometries and potential arch materials to give baseline data on the local compressive buckling capacity that can be used to verify analytical and numerical models of wall buckling and assist in checking the capacity of an arch during concrete filling.

Specimen Fabrication and Material Properties

Fabricating Tubes

Laminate structure and the number of specimens tested for each type is listed in Table 11. Specimen identification begins with fiber composition; SC was a single carbon structural layer with a glass layer; BC was a single carbon structural layer, an outer bleeder abrasion resistance layer, and a glass layer; and DC was two layers of carbon with a glass layer. The second identifier was the nominal diameter of the specimen, 6.50in (165mm), 11.8in (300mm), or 14.8in (375mm); for example BC 300 refers to a 11.8in diameter bleeder carbon tube. For specimens with holes a third identifier was hole diameter, either 1.77in (45mm) or 3.00in (76mm); for example, BC 165-45 refers to a 6.50in diameter bleeder carbon tube with a 1.77in diameter hole. For a group of specimens tested with a known defect of inconsistent diameter, ID was added to the specimen label (SC 300-ID). Table 11 contains minimum buckling load, maximum buckling load, average buckling load, and COV of loads for each specimen type. Loads will be discussed in further detail in the failure strength section.

This test report shall not be reproduced, except in full, without the written approval of
the AEWC Advanced Structures & Composites Center.

Table 11 Compressive Testing Matrix

	SC 165	DC 165	B.C 165	DC 165-45	DC 165-76	BC 165-45	BC 375	BC 375-76	SC 300	BC 300	SC 300-ID
Diameter (in)	6.50	6.50	6.50	6.50	6.50	6.50	14.8	14.8	11.8	11.8	11.8
Height (in)	15.0	15.0	15.0	15.0	15.0	15.0	29.9	29.9	18.1	18.1	18.1
Layers of Carbon	1	2	1	2	2	1	1	1	1	1	1
Carbon Layer Thickness (in)	.027	.027	.027	.027	.027	.027	.038	.038	.03	.03	.03
Carbon Braid Angle (deg)	22	22	22	22	22	22	18	18	22	22	22
Glass Thickness (in)	.035	.035	.035	.035	.035	.035	.039	.039	.046	.046	.046
Glass Braid Angle (deg)	81	81	81	81	81	81	76	76	81	81	81
Bleeder Thickness (in)	–	–	.03	–	–	.03	.035	.035	–	.03	–
Hole Diameter (in)	–	–	–	1.77	2.99	1.77	–	2.99	–	–	–
Hole to Diameter Ratio	–	–	–	0.273	0.461	0.273	–	0.203	–	–	–
Known Defect	No	No	No	Yes	Yes	Yes	No	Yes	No	No	Yes
Number of Specimen Tested	37	10	14	9	8	14	4	4	6	5	7
Number Included in Results	22	8	12	9	7	11	4	4	6	5	7
Average Ultimate Load (kip)	15.5	30.8	23.2	16.7	10.7	11.1	31.9	19.4	19.9	29.0	13.8
COV (%)	18.5	5.07	13.4	5.69	7.45	7.76	17.0	30.4	18.4	17.4	5.80
Lowest Ultimate Load (kip)	10.8	27.7	18.4	15.3	9.51	9.71	28.1	10.7	14.8	24.7	12.9
Highest Ultimate Load (kip)	21.4	33.0	27.0	17.9	11.8	12.1	39.8	23.2	25.2	35.3	15.0

This test report shall not be reproduced, except in full, without the written approval of the AEWC Advanced Structures & Composites Center.

All tubes used for testing were fabricated at AEWC. Arches used for bridges and fill testing as part of this research were fabricated by Kenway Corporation in Augusta, Maine. Arches are manufactured through the vacuum assisted resin transfer molding (VARTM) process, where vacuum suction forces the resin onto the fibers. This technique produces composites with a relatively high fiber volume fraction, little excess resin, and during VARTM there is little exposed resin reducing expelled gasses in the work area. Derakane vinyl ester 8084 resin was used in all specimens.

Arches are multilayer hybrid braided composites; each arch comprises two or more total layers and typically has a layer of braided glass fiber and at least one layer of braided carbon fiber. Braided fabrics keep all fibers aligned at the same angle (positive and negative) and allow layers to be pulled atop one another as a sock. The inner layer of a tube or arch is braided e-glass with fibers arranged close to the transverse or hoop direction (75 to 81 degrees relative to the longitudinal arch axis depending on diameter).

Outer layers of the tube, longitudinal strength layers, are comprised of fibers arranged closer to the longitudinal direction (15 to 30 degrees measured from the longitudinal arch axis for the tested specimens). Tubes have been constructed with one or two layers for this research, although additional layers have been used before, and outer layers for test specimens have been either carbon or glass fiber. All arches manufactured for bridges or built as direct replicas of bridge fiber architecture have been built with carbon fiber only for the longitudinal structural layers.

In some circumstances an additional 'bleeder' layer was added to the tubes. This layer is a thin (~0.028in) polyester random-orientation blanket material commonly used in composite manufacture to slow resin flow while keeping air passages open near vacuum ports. Originally added as an abrasion resistant layer, the bleeder material also helps local buckling capacity because it adds to the thickness of the cylinder. The bleeder has much lower stiffness than the longitudinal direction of the fibers, so it only minimally changes the longitudinal stiffness (elastic modulus times thickness) but it substantially changes the radial stiffness, or resistance to cross sectional shape change, as that term depends on thickness cubed; local buckling is a failure of the cross sectional integrity.

Material Assumptions

Throughout this thesis certain material properties, E_x-longitudinal elastic modulus, E_θ-radial elastic modulus, ν_{xy}-Poisson's ratio, G_{xy}-shear modulus, were predicted for comparison with experimental results or to use in models when no experimental properties existed for that laminate. Classical Lamination Theory (CLT) with micromechanics was used to calculate all of these properties (for further information on

This test report shall not be reproduced, except in full, without the written approval of
the AEWC Advanced Structures & Composites Center.

Classical Lamination Theory and micromechanics see Daniel and Ishai (2006)). Micromechanics provides a method of combining the properties of the vinyl ester resin with the fiber (carbon, glass, polyester bleeder) to get combined orthotropic properties, input properties are in Table 12. For transverse modulus and shear modulus the Halpin-Tsai approximations were used (Daniel and Ishai, 2006). Fiber volume fraction, V_f, is calculated from material properties explained later in this section.

Table 12 Micromechanics Constituents

Properties	**Matrix**	**E-Glass Fiber**	**Carbon Fiber**	**Bleeder Fabric**
V_f	-	0.56	0.56	0.33
***E* (Ksi)**	421	10400	34800	1450
***G* (Ksi)**	160	4350	4061	580
v	0.35	0.23	0.20	0.30

Classical Lamination Theory assumes a laminate comprises a stack of unidirectional plies. A braided layer is different from a unidirectional layer and the interaction of fiber and matrix are more complex in a braid. Several authors, including (Zeng et. al. 2004 Chen et. al. 1999 and Lei et. al. 1992), have addressed material properties of a braided composite with sophisticated finite element models. While these values can predict both strength and elastic properties, the purpose of material modeling in this thesis is to acquire missing elastic properties only, not predict composite capacity, because compression buckling failure results from a different mechanism than fiber failure.

When using CLT, braided fabrics do not achieve as high longitudinal elastic modulus as uniaxial plies (Carey, 2003), resulting in over prediction of stiffness. An approximation developed by Cox and Dadkhah (1995) based on a sinusoidal wave shape beam gives a longitudinal stiffness reduction factor. In Equation 2
, t_f is the fiber thickness, λ is the wavelength (measured at .709in for the carbon), E_1 is the fiber elastic modulus in the fiber direction, G_{12} is the in-plane shear modulus, v_{12} is the Poisson's ratio.

$$E_1(wavy) = E_1\left(1 + 2\left(\frac{t_f \pi}{\lambda}\right)^2\left(\frac{E_1}{G_{12}} - 2(1 - \nu_{12})\right)\right)^{-1} \qquad \text{Equation 2}$$

Later research (Edgren and Asp 2005) suggests that this model does not perfectly approximate the material stiffness. However, this model showed good agreement with results of coupon-level stiffness tests conducted at the University of Maine on carbon

This test report shall not be reproduced, except in full, without the written approval of
the AEWC Advanced Structures & Composites Center.